AD-A041 413 PROTOTYPE DEVELOPMENT ASSOCIATES INC SANTA ANA CALIF F/G 11/4
A GENERAL THREE-DIMENSIONAL COMPUTATIONAL MODEL FOR NONLINEAR C--ETC(U)
JUN 77 E L STANTON N00014-76-C-0161
UNCLASSIFIED PDA-TR-1045-00 NL

| OF |
AD
A041413

END
DATE FILMED
8-77

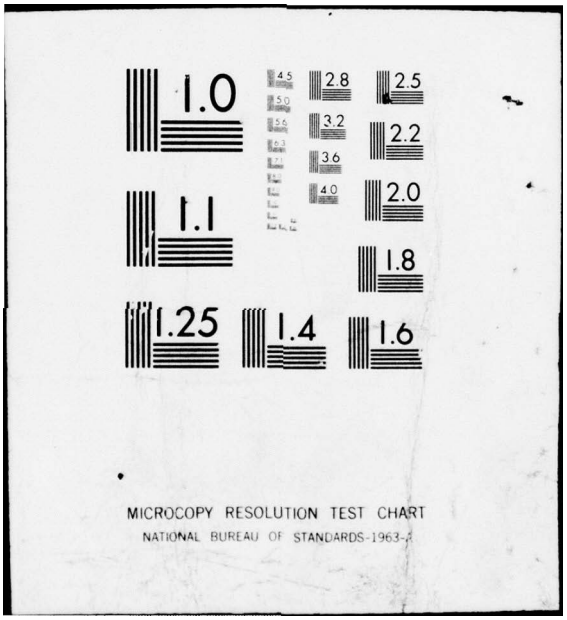
1.0
1.1
1.25
1.4
1.6
1.8
2.0
2.2
2.5
2.8
3.2
3.6
4.0
4.5
5.0
5.6
6.3
7.1
MICROCOPY RESOLUTION TEST CHART
NATIONAL BUREAU OF STANDARDS-1963-

# A GENERAL THREE-DIMENSIONAL COMPUTATIONAL MODEL FOR NONLINEAR COMPOSITE STRUCTURES AND MATERIALS



Edward L. Stanton

PROTOTYPE DEVELOPMENT ASSOCIATES, INC.
1740 Garry Avenue, Suite 201
Santa Ana, California 92705

June 1977

Prepared for
OFFICE OF NAVAL RESEARCH
Contract No. N00014-76-C-0161



PDA, inc.
PROTOTYPE DEVELOPMENT ASSOCIATES

Ref 9 - two corrections to
- 1045 - for the author.
(914) 556-2550
Lyn Crumbacher
12A - 11 Jul 79

PDA TR 1045-00

# A GENERAL THREE-DIMENSIONAL COMPUTATIONAL MODEL FOR NONLINEAR COMPOSITE STRUCTURES AND MATERIALS

June 1977

Prepared by

Edward L. Stanton

PROTOTYPE DEVELOPMENT ASSOCIATES, INC.
1740 Garry Avenue, Suite 201
Santa Ana, California 92705

# FOREWORD

A general three-dimensional computational model for nonlinear composite structures and materials was developed by Prototype Development Associates, Inc. (PDA) under Contract Number N00014-76-C-0161 for the Office of Naval Research. Dr. E. L. Stanton served as Program Manager, Mr. L. M. Crain was responsible for scientific programming services, Dr. D. Mulville served as technical monitor for the Navy and Dr. J. Buch of PDA contributed a wealth of background information on material behavior. Their support and that of Dr. N. Perrone, who originated the project, are gratefully acknowledged.

## ABSTRACT

A computational model for the analysis of structural and microstructural behavior in general solids of composite material is presented. Emphasis is placed on representing the anomalous material behavior of composites and on the construction of computational models with variable properties. Alternative material models using continuum and statistical mechanics were reviewed and a modular code designed for compatibility with several different models. The constituent materials are characterized in terms of those state variables that correlate a materials response such as effective stress or strain energy. A parametric cubic representation is used for all state variables, the solid geometry and all physical properties. The associated finite element extends isoparametric modeling to allow properties, linear or nonlinear, to vary over the volume of an element as in rosette material construction. Applications of the model to a carbon-carbon unit cell, to strain singularities and to the inelastic response of a graphite bar illustrate its utility. Good agreement with triaxial test data for inelastic strains under hydrostatic pressure is obtained. Numerical results are computed using PATCHES-III and the conjugate gradient algorithm without the assembly of large matrices. This approach is tailored for vector processors and can reduce the high cost of nonlinear three-dimensional analyses.

## NOMENCLATURE

| | |
|---|---|
| $a$ | Penny shaped crack radius |
| $B_i$, $B_{ij}$ | Parametric cubic line and surface patch coefficients in geometric format |
| $\underset{\sim}{B}$ | Binormal vector in the Frenet frame for a curve |
| $C_{ijkl}$ | Stress-strain coefficients |
| $\Delta C_n$ | Difference in $C_{ijkl}(O, T)$ and $C_{ijkl}(V_n, T)$ |
| $c^o$ | Scalar multiplier in the Batdorf model |
| $\underset{\sim}{e}_i$ | Cartesian basis vector |
| $E_L$, $E_T$ | Longitudinal and transverse extensional moduli |
| $F_{ij}$, $F_{ijkl}$ | Material strain state coefficients |
| $\overline{F}_{ij}$, $\overline{F}_{ijkl}$ | Material stress state coefficients |
| $\underset{\sim}{F}$ | Applied load vector |
| $G_{LT}$, $G_{TT}$ | Shear moduli in the longitudinal-transverse plane and the transverse plane |
| $[K]$ | Stiffness matrix |
| $n$ | Index indicating cycle number |
| $N$ | Dimension of a matrix problem |
| $\underset{\sim}{N}$ | Normal vector in the Frenet frame for a curve |
| P.E. | Potential energy |
| $P(\xi)$ | Parametric cubic property model |
| $\underset{\sim}{P}$ | Conjugate gradient direction vector |
| $\underset{\sim}{Q}_n$ | Pseudo-force vector at cycle n |
| $r$ | Radius |
| $\underset{\sim}{R}$ | Residual vector |
| $S_i$, $S_{ij}$ | Parametric cubic line and patch coefficients in algebraic format |
| $t_i$ | Conjugate gradient step size at cycle i |
| $\underset{\sim}{T}$ | Tangent vector in the Frenet frame for a curve |
| $T$ | Temperature |
| $\underset{\sim}{u}$ | Displacement vector at a point |

| | |
|---|---|
| $V_i$ | Variable representing a material strain state |
| $\overline{V}_i$ | Variable representing a material stress state |
| $W$ | Strain energy density |
| $Z_i$ | Coordinate i in the $\underset{\sim}{e}_i$ frame |
| $Z(\xi)$ | Parametric cubic line |
| $\alpha_L, \alpha_T$ | Longitudinal and transverse thermal expansion coefficient |
| $\alpha_{ij}$ | Coefficients of thermal expansion |
| $\beta_i$ | Conjugate gradient direction factor |
| $\epsilon_{ij}$ | Strain components |
| $\theta$ | Polar coordinate angle |
| $\xi_i$ | Parametric coordinate $0 \leq \xi_i \leq 1$ |
| $\sigma$ | Effective stress |
| $\sigma_i^o$ | Normalizing stresses in the Batdorf model |
| $\sigma_{ij}$ | Stress components |
| $\varphi$ | Helix angle |
| $\omega$ | Over-relaxation factor |

TABLE OF CONTENTS

LIST OF FIGURES

LIST OF TABLES

## 1.0 INTRODUCTION

The use of composite materials for primary structure has led to demands for information on their three-dimensional response simply because uniaxial and biaxial loading often lead to important triaxial effects. This is true in the elastic range where edge effects can cause delamination and it is particularly true in the inelastic range where load redistribution can be strongly dependent on the microstructure of the material. One of the more readable essays on this subject is Drucker's[1] account in words and pictures of how different microstructures effect inelastic macroscopic response. Many of these involve inelastic mechanisms quite different from the crystallographic slip characteristic of metals. Some graphites exhibit biaxial softening due in part to microcracking[2] and several correlative models[3,4] (i.e., phenomenological) are available that fit this data in the tension-tension quadrant. Quite the opposite behavior can occur in the compression-compression quadrant for another particulate composite, concrete, where the confinement of microcracks results in biaxial stiffening and again correlative models[5] are available that fit this data. Anomalous inelastic behavior also occurs in fiber-reinforced composites as described in the survey paper by Francis and Bert[6] who review the history of the fiber-matrix load transfer controversy. This issue is complicated by microstructural defects, particularly in composites subjected to severe processing conditions, by local fiber buckling and by residual processing strains.

Genuinely predictive inelastic models for composite materials are not available and most correlative models are an extrapolation of uniaxial data to multiaxial stress states. The situation in metals is similar[7] but not to the same degree. Lin[8] and Havner[9], for example, have produced models that can predict multiaxial stress-strain response for polycrystalline aggregates and microstructural models at the atomic level[10] (lattice statics) are also used in the material sciences. The microstructural detail required in a predictive material model for inelastic response clearly can be prohibitive for structural mechanics. In the case of composite

materials even the assumption of a statistically homogeneous material may not hold for certain behavior. However, when it does apply and when the principle of local action applies, we can use correlative models supported by adequate testing for structural mechanics. Operationally, this may require one or more pre-processors to obtain a correlative model and one or more post-processors to obtain results at the constituent level. Given this premise, the present effort focused on developing a computational system for all those correlative models that can be characterized by state variables. This is a very large class and will allow the numerical analysis of many composite structures whose inelastic behavior differs from metal plasticity. The approach also allows the model to function as its own pre-processor and synthesize correlative models from constituent inelastic properties and the behavior at interfaces.

The magnitude of the computational problem associated with inelastic three-dimensional analyses approaches that of characterizing the materials' physics. Several excellent survey papers are available[11] as well as case histories of recent applications.[12] The computational approach taken in the present paper is based on the premise that better computers are more likely than better numerical methods. Consequently, a computational method was adopted that takes advantage of what most scientific computers do best, vector processing. It is an adaption of the conjugate gradient algorithm that avoids connectivity optimization, that uses relatively little core and whose cycle time grows at most linearly. One of the method's disadvantages in linear problems, it is inefficient for multiple load conditions, can become an advantage in nonlinear problems when the iteration for the next load increment is started from the solution for the previous increment. A second aspect of the computational problem is that of data generation for the discrete mathematical model. This problem received considerable attention in the original development of PATCHES-III and resulted in a parametric cubic modeling system based on construction-in-context.[13] The present effort added new geometry construction operations to the system, developed the parametrization necessary for modeling strain singularities, developed intra-element

property modeling and developed a common input format for all nonlinear material properties. Applications of these features are made to a carbon-carbon unit cell, to an interior crack problem and to the triaxial response of a graphite bar tested by Jortner.[2]

## 2.0 MATERIAL MODELS

### 2.1 State Variable Models

The objective is a general computational model that accounts for the anomalous inelastic behavior of composite materials, Table 1. The basic assumptions are that the material is statistically homogeneous and that at the macroscopic level inelastic behavior is strictly local. It is also tacitly assumed that this behavior is deterministic which may be the weakest link in the chain of assumptions. Physically based statistical models[14] have been very successful in explaining the extensional behavior of graphites associated with the nucleation and growth of microcracks. However, additional work is required to include a shear mechanism and to reduce their computational expense before they can serve as the basis for a general computational model. Mathematically based statistical theories have not been nearly as successful.

Table 1 Anomalous inelastic behvior observed in composites

| Behavior | Metals | Composites |
|---|---|---|
| Yielding | Independent of hydrostatic stress | Can be dependent on hydrostatic stress |
| Inelastic Mechanism | Crystallographic slip Twinning | Microcracking, interstitial slip, microbuckling |
| Inelastic Strain | Constant volume plastic strains | Inelastic strains can cause volume changes |
| Unloading | Occurs at elastic modulus | Can occur at secant modulus |
| Failure | Convex failure surfaces | Concave failure surfaces can occur |

The approach taken assumes simply that the stress-strain law is some function of one or more stress or strain state variables. This assumption can be used for both incremental and total stress-strain laws but the present effort is limited to the latter and to three state variables

$$\sigma_{ij} = C_{ijkl}(V_1, V_2, T)\, \epsilon^{M}_{kl} \tag{1}$$

where one is temperature and $\epsilon^{M}_{kl}$ is the mechanical strain. Although not prescribed, commonly used $V_1$ and $V_2$ expressions are

$$V_1 = F_{ij}(V_1, V_2)\, \epsilon^{M}_{ij}$$

and

$$V_2 = F_{ijkl}(V_1, V_2)\, \epsilon^{M}_{ij}\, \epsilon^{M}_{kl} \tag{2}$$

with analogous expressions for strain-stress formulations



$$\bar{V}_1 = \bar{F}_{ij}(\bar{V}_1, \bar{V}_2)\, \sigma_{ij}$$

$$\bar{V}_2 = \bar{F}_{ijkl}(\bar{V}_1, \bar{V}_2)\, \sigma_{ij}\, \sigma_{kl} \tag{3}$$

There is a formal similarity to the nonlinear stress-strain model of Nueber[15], but his model restricts the form of Equation (1) and does allow the coefficients in Equations (2) and (3) to be independent functions of the state of the material. This is necessary to account for changes in the degree of anisotropy during inelastic straining.[16, 17] A great many correlative models including Batdorf, Jones-Nelson, Weiler, Hahn-Tsai and the classical deformation models can be represented using Equation (1). It allowed the design of a nonlinear material module encompassing a variety of formulations all using one input format. All moduli and state functions are interpolated using piecewise cubics which are capable of approximating any continuous function as closely as required. This avoids the interpolation problems associated with exponential approximations in the Jones-Nelson model. The state variable used in this model is the strain energy density, $V_2 = W$, so that the $F_{ijkl}$ are the $C_{ijkl}$ and the nonlinear equation

$$W = C_{ijkl}(W)\, \epsilon^{M}_{ij}\, \epsilon^{M}_{kl} \quad \text{(Jones-Nelson)} \tag{4}$$

must be solved for each strain state. The Batdorf model is a strain-stress formulation that is very simple and accurate for transversely isotropic graphites. It uses an

effective stress parameter for a state variable that can be converted to a strain formulation by solving a nonlinear equation.

$$\bar{\sigma}^2 = \bar{F}_{ijkl}\,\sigma_{ij}\,\sigma_{kl} \quad \text{(Batdorf)}$$

$$= \bar{F}_{ijkl}\,C_{ijmn}\,(\bar{\sigma})\,C_{klst}\,(\bar{\sigma})\,\epsilon^{M}_{mn}\,\epsilon^{M}_{st} \tag{5}$$

The moduli are linearly dependent on $\bar{\sigma}$ in this model. In order to account for tension-compression behavior differences, Batdorf uses an ad hoc procedure based on the sign of individual stress components. Unfortunately, this procedure, when used with Equation (5), often will lead to oscillating divergence between two stress states having the same $\bar{\sigma}$ but different signs. To avoid this, the signs are held constant during each major cycle in PATCHES-III. These difficulties are rewarded by surprisingly accurate agreement with the extensive biaxial and triaxial data obtained by Jortner.[2] Numerical results obtained using Equation (5) are compared with his data later in the paper for triaxial loading at constant strain ratios.

The Weiler model also uses an effective stress parameter for a state variable but allows the $\bar{F}_{ijkl}$ to be dependent on the effective stress to account for changes

$$\bar{\sigma}^2 = \bar{F}_{ijkl}\,(\bar{\sigma})\,\sigma_{ij}\,\sigma_{kl} \quad \text{(Weiler)} \tag{6}$$

in anisotropy with strain. The procedure used by Weiler and others[18] is based on constraining the effective plastic work to be equal to the uniaxial plastic work in each component. Applications of these models have used $\bar{F}_{ijkl}$ functions that make the effective stress insensitive to hydrostatic pressure, but this is not a requirement. Rybicki[19] included plastic volume change in an $\bar{F}_{ijkl}$ model for a carbon material, JTA, several years ago and obtained good correlation with data for a pressurized test cylinder under axial load. He, too, used an ad hoc procedure to account for tension compression differences.

The correlative models described have been used principally for particulate composites. It is also possible to represent most correlative models used

for fiber reinforced composites with Equation (1). Consider for example the Hahn-Tsai[20] model in which the nonlinearity for a laminar is shear dominated. In this case

$$V_2 = \bar{F}_{1212}\ \sigma_{12}^{\ 2} \qquad \text{(Hahn-Tsai)} \tag{7}$$

and the extensional $C_{ijkl}$ are independent of $V_2$. There are essential differences between this model and those using strain energy for $V_2$ although at small strain levels both fit the data for graphite-epoxy laminates reasonably well.[21]

2.2 Spatial Variable Models

The objective is to model property distributions as accurately as deformations so that modeling detail is controlled by representation of the output rather than the input. This requirement is another instance in which composite material modeling differs from metals both for microstructures and structures. A carbon-carbon unit cell, for example, can be modeled with one variable property element or eight constant property elements. A helically wound structure with changing radii has properties that are continuously changing and is also most efficiently modeled with variable property elements. The approach taken in PATCHES-III is to use the same parametric cubic functions for both geometry and physical data. It is a generalization of the isoparametric approach and requires the development of new modeling techniques for properties.

Recently Henshell[22] demonstrated how variable mesh point spacing (parametrization) can be used to greatly improve isoparametric models near a strain singularity. The same technique, changing the parametrization of the geometry model, can be used to model the step in material properties at an interior bimaterial interface. In this instance, Figure 1, we induce an inflection point in the property model at the interface by constructing a geometry model with an inflection point at the interface. Consider a coordinate function $Z(\xi)$ in algebraic format

$$Z(\xi) = S_1 \xi^3 + S_2 \xi^2 + S_3 \xi + S_4 \tag{8}$$

and impose the boundary conditions and inflection constraint

$$
\begin{aligned}
Z(0) &= S_4 \\
Z(1) &= S_1 + S_2 + S_3 + S_4 \\
\dot{Z}(\bar{\xi}) = 0 &= 3\,S_1\,\bar{\xi}^2 + 2\,S_2\,\bar{\xi} + S_3 \\
\ddot{Z}(\bar{\xi}) = 0 &= 6\,S_1\,\bar{\xi} + 2\,S_2
\end{aligned}
\tag{9}
$$

where the step is at $\bar{Z} = Z(\bar{\xi})$. Next solve Equations (9) in terms of the as yet unknown $\bar{\xi}$ where $\Delta Z = Z(1) - Z(0)$.

$$
\begin{aligned}
S_1 &= \Delta Z \,/\, \left(3\bar{\xi}^2 - 3\bar{\xi} + 1\right) \\
S_2 &= -3\Delta Z\,\bar{\xi} \,/\, \left(3\bar{\xi}^2 - 3\bar{\xi} + 1\right) \\
S_3 &= 3\Delta Z\,\bar{\xi}^2 \,/\, \left(3\bar{\xi}^2 - 3\bar{\xi} + 1\right) \\
S_4 &= Z(0)
\end{aligned}
\tag{10}
$$

The location of the step or interface in parametric space, $\bar{\xi}$, can now be found by solving the cubic equation

$$
\bar{\xi}^3 - 3\,(\overline{\Delta Z}/\Delta Z)\,\bar{\xi}^2 + 3\,(\overline{\Delta Z}/\Delta Z)\,\bar{\xi} - (\overline{\Delta Z}/\Delta Z) = 0 \tag{11}
$$

for the root in the interval $0 \le \bar{\xi} \le 1$ where $\overline{\Delta Z} = \bar{Z} - Z(0)$ and Descartes' rule of signs guarantees there will be a root in the interval. Finally, a parametric cubic for a property component $P(\xi)$ is obtained by imposing the boundary conditions $P(0) = P_o$, $P(1) = P_1$ and $\dot{P}(0) = \dot{P}(1)$. Other choices are possible, for example, the value of $P(\xi)$ could be prescribed at four points, but this will cause $P(\xi)$ to fall outside the interval $\left[P_o,\ P_1\right]$ over portions of the interval $0 \le \xi \le 1$. This may be necessary if the area under the curve is a key parameter. One might keep the $\dot{P}(0) = \dot{P}(1) = 0$ constraint and choose the value of $P(0)$ such that the integral of $P(\xi)$ on the interval $0 \le \xi \le \bar{\xi}$ gives the correct area, $P_o\overline{\Delta Z}$, with the corresponding choice for $P(1)$. In general, the determination of the parametrization and the intra-element property model form a nonlinear programming problem once an accuracy criteria such as least squares is established. However, a great deal can be accomplished with

simple analyses of the type presented. Parametrizations for a strain singularity at Z (0), for example, can be obtained without solving a cubic and several are listed in Table 2.

Table 2 Strain singularity parametrizations

| $Z(\xi)$ | $Z(0)$ | $Z(1/3)$ | $Z(2/3)$ | $Z(1)$ |
|---|---|---|---|---|
| $\xi^2$ | 0 | L/9 | 4L/9 | L |
| $\xi^3$ | 0 | L/27 | 8L/27 | L |
| $\xi^2+\xi^3$ | 0 | 4L/27 | 20L/27 | L |

Consider next the modeling of a fiber reinforced structure in which the orientation of the material axes changes continuously with respect to a reference frame. An interesting example is rosette construction used in rocket nozzle structures in which the fibers spiral about an axis with changing radii, Figure 2. Pagano[23] provides a detailed account of the relations between coordinate frames and shows that while axisymmetric, the properties vary in the radial direction. Also, all 21 elastic constants are non-zero for this material in cylindrical or rectangular coordinates making efficient property modeling particularly important. The transformation from material coordinates to cylindrical coordinates in this case is determined by a rotation $\varphi$ = constant followed by a rotation $\alpha = \alpha(r)$ where r sin $\alpha$ = constant. The transformation to rectangular coordinates simply requires adding a rotation $\Theta$ to $\alpha$. Intra-element property modeling in this case requires only the ply properties and the spatial distribution of the Euler angles. The original PATCHES-III system was designed for such input but did not anticipate the need for variable Euler angle data. As a result, the spatial variation of all 21 elastic constants had to be modeled individually using a pre-processor for a one-element model of a rosette cylinder. The same model could have been created

from the spatial variation of three Euler angles, two of which are constant. Comparisons between the parametric cubic properties and the analytic showed differences of less than one percent. Complete results from this study will be presented in a later paper. Finally, it should be remembered that variable property modeling adds no new degrees-of-freedom to the analysis model and can reduce the number of elements required for some composite materials.

## 3.0 COMPUTATIONAL MODELS

### 3.1 Geometry

The basic constructions and properties for parametric cubic line, surface and volume models may be found in the work of Coons[24] and others[13]. They provide a data base for computer aided geometric design comprehensive enough to be used for parts definition in manufacturing[25] and they now are used extensively in industry here and abroad to define external surfaces. Their reliability derives from modeling in parametric space where there are no problems with asymptotic slopes and their accuracy derives from using Hermite polynomials which interpolate a function and its derivatives with the smallest possible error. The price for these qualities is twelve coefficients for a line, forty-eight for a surface patch and one hundred ninety-two for a volume hyperpatch. The data generation problem for these coefficients can be solved using the construction-in-context approach developed originally for PATCHES-III. This system uses a variety of LINE___, PATCH___ and HP___ directives with cross referencing to construct the geometry model. Two construction operations, ruled volume and outline surface, are illustrated in Figure 3 and a listing of the currently available options is provided in Table 3. The outline surface construction operation shown in Figure 3 consists in having the computer move an outline curve along a base curve with a fixed orientation relative to either a global Cartesian frame or the local Frenet frame of the base curve. In developing this option, it became obvious that in many instances it would be desirable to change the initial orientation of the outline curve. This feature was provided by allowing an initial transformation that leaves the file copy of the outline curve unchanged. In retrospect, many of the original PATCHES-III directives would have benefited from such a feature which functions as a modifier in the language implicit to the present approach. The benefits of having even a primitive language have been substantial for data generation. The system functions as its own pre-processor and allows shapes, like those shown in Figure 4, to be created using roughly ten input directives (cards) per model. However, the models created contain several hundred coefficients that completely describe the geometry of the figure. The Frenet frame for a line $Z(\xi)$, for example, can be computed directly from the parametric cubic model

$$\underset{\sim}{T} = \dot{\underset{\sim}{Z}} / |\dot{\underset{\sim}{Z}}|$$
$$\underset{\sim}{N} = \ddot{\underset{\sim}{Z}} / |\ddot{\underset{\sim}{Z}}|$$
$$\underset{\sim}{B} = \underset{\sim}{T} \times \underset{\sim}{N} \qquad (12)$$

where the dot indicates differentiation with respect to, $\xi$, the parametric coordinate. It is also a routine matter to compute surface normals, areas, volumes, curvatures and in short any geometric property.

Table 3 Geometry construction directives*

| | | | |
|---|---|---|---|
| LARCPC | PATCHB | HPB | SCALP |
| LINEB | PATCHGR | HPL | SCALPH |
| LINECS | PATCHL | HPHEX | TMOVE |
| LINEPC | PATCHO | HPN | |
| | PATCHQ | HPP | |
| | PATCHR | HPR | |
| | | HP2PAT | |
| | | HP6PAT | |

* Mnemonic Suffixes:

A = Algebraic , B = Geometric , CS = Cubic Spline, L = Line,
N = Normal , P = Point , PC = Parametric Cubic ,
Q = Quadrilateral , R = Rotation ,

## 3.2 Finite Element

The decision to use the sixty-four point isoparametric finite element for the present study rests on its modeling efficiency for anisotropic materials, for pathological shapes and for general boundary conditions. There are many cases in which these qualities are not required; however, the focus here is on the anomalous behavior of composites particularly in highly stressed states. In this regard it is important to realize that material anisotropy affects matrix conditioning as strongly as geometric aspect ratio. Consider, for example, a heated disk with isotropic properties (E/G = 2.6) and with highly anisotropic properties (E/G = 17.25) in which the temperature varies quadratically with radius. This change in material anisotropy

caused the number of elements required for good stresses to double as Table 4 demonstrates. The large hoop stress ratio at $r = 2R/3$ is near a $\sigma_\theta = 0$ point

Table 4 Anistotropy effects on stress accuracy

| | Isotropic Two Elements | | Anisotropic Two Elements | | Anisotropic Four Elements | |
|---|---|---|---|---|---|---|
| r/R | $\sigma_r$* | $\sigma_\theta$* | $\sigma_r$* | $\sigma_\theta$* | $\sigma_r$* | $\sigma_\theta$* |
| 0 | .998 | .998 | 1.128 | 1.128 | 1.033 | 1.033 |
| 1/3 | .981 | .977 | .841 | 1.142 | 1.035 | 1.045 |
| 2/3 | .977 | 1.030 | .461 | .597 | .901 | 1.365 |
| 1 | ** | .998 | ** | .473 | ** | 1.099 |

* Ratio of computed stress to exact stress
** The exact stress is zero at this point

and is simply an indication of large differences in small numbers. Similar studies on the effect of high aspect ratios and degenerate element shapes indicate the sixty-four point element has a broad band over which it can maintain good stress accuracy. In order to realize these benefits many practical problems associated with large element matrices had to be solved in the original PATCHES-III system and the added burden of material nonlinearity required similar efforts.

An examination of the relative costs of generating an element stiffness matrix vs. generating an element thermal load vector for a carbon-carbon material range from 40:1 to over 90:1 depending on the geometry. These ratios are very high in comparison to lower order elements and strongly suggest the use of a pseudo-force formulation for material nonlinearity. When direct matrix solution methods are used, another factor in favor of this approach is the ratio of matrix assembly and decomposition time to the forward-backward solution time which is typically 6:1. The computational factors in favor of an initial stress formulation are faster convergence and greater stability at high strain levels. Studies of the relative convergence rates by Havner[26] indicate roughly 2:1 ratios in favor of the initial stress method which is not nearly enough to make the method competitive. Stability will not be a factor for small strains and a periodic initial stress cycle can always be taken if necessary.

There are many derivations of the matrix equations associated with the pseudo-force method and they need not be repeated here. The matrix equations used in the present study are very similar to those used by Havner.[26]

$$[K(V, T)]\ \underset{\sim}{U} = \underset{\sim}{F}$$

$$[K(O, T)]\ \underset{\sim}{U} = \underset{\sim}{F} + [K(O, T) - K(V, T)]\ \underset{\sim}{U} \tag{13}$$

which leads to the recursion relations

$$[K(O, T)]\ \underset{\sim}{U}_{n+1} = \underset{\sim}{F} + [K(O, T) - K(V_n, T)]\ \underset{\sim}{U}_n$$

$$[K(O, T)]\ \underset{\sim}{U}_{n+1} = \underset{\sim}{F} + \underset{\sim}{Q}_n \tag{14}$$

The pseudo-force term is obtained by integrating the strains from cycle n against the difference in properties referring to Figure 5

$$\underset{\sim}{Q}_n = \int_V [B]^T [\Delta C_n]\ \underset{\sim}{\epsilon}_n dV \tag{15}$$

where [B] transforms mesh point displacements $\underset{\sim}{U}$ into strains.

A sufficient condition for convergence of the method inferred from Havner's analysis is that $[K(V, T)]$ must be monotonic in V. It should be noted that in material models with inelastic volume changes, the body forces for thermal stress problems will also change. These change can be accounted for in $Q_n$ by using the mechanical strains in Equation (15). The limited experience to date with the method has enjoyed rapid convergence. As more complex problems are attempted, it may be necessary to utilize more efficient recursion relations. Another method that was considered in the study casts the problem in the form of a first order differential equation using the residual vector formed from Equation (14).

$$\underset{\sim}{R} = -[K]\underset{\sim}{U} + \underset{\sim}{F} - \underset{\sim}{Q} \tag{16}$$

$$\dot{\underset{\sim}{R}} + \omega\underset{\sim}{R} = \underset{\sim}{Q} \tag{17}$$

The dot indicates a time derivative where time increments are synonymous with load increments and the scalar $\omega$ is equivalent to an over-relaxation factor. Stricklin, et al.[27] use this approach to derive a self-correcting procedure that worked very well in their nonlinear material applications.

### 3.3 Matrix Solution

The third major computational problem after data generation and matrix generation is matrix solution. The use of a 64-point finite element leads to matrix equations that are relatively dense. It is not unusual for densities of 35 percent to occur in matrices well over dimension 1000. The original linear code development concentrated on the first two computational problems and used existing (NASTRAN) matrix routines to solve the matrix equations. As a result, the system is efficient for problems up to about dimension 1000 and looses efficiency for larger matrices until eventually saturating the computer. The need to solve similar dimension nonlinear matrix equations led to a change to an iterative solution method. The advantages of this change are 1) elimination of large matrix files, 2) freedom from connectivity optimization problems, 3) relatively small core requirements for large problems and 4) heavy vector processing. The disadvantages are possible slow convergence and, in linear problems, N multiple-load conditions are N times as expensive as one. The iterative method selected is the conjugate gradient algorithm[28]

and in properly scaled coordinates, it converges in far fewer cycles than the dimension of the matrix. Referring to Equation (16) for the residual $\underset{\sim}{R}$

$$\begin{aligned} \underset{\sim}{P}_0 &= \underset{\sim}{R}(\underset{\sim}{U}_0) \\ \underset{\sim}{U}_{i+1} &= \underset{\sim}{U}_i + t_i \underset{\sim}{P}_i \\ \underset{\sim}{P}_{i+1} &= \underset{\sim}{R}(\underset{\sim}{U}_{i+1}) + \beta_i \underset{\sim}{P}_i \end{aligned} \tag{18}$$

where the scalers $t_i$ and $\beta_i$ are

$$\begin{aligned} t_i &= |\underset{\sim}{R}_i|^2 \; / \; \underset{\sim}{P}_i^T [K] \underset{\sim}{P}_i \\ \beta_i &= |\underset{\sim}{R}_{i+1}|^2 \; / \; |\underset{\sim}{R}_i|^2 \end{aligned} \tag{19}$$

This is the linear form of the algorithm appropriate to the solution of Equation (14). It is also possible to use the nonlinear version of the algorithm to solve Equation (13) directly. In this case, $t_i$ is the smallest positive root of $\underset{\sim}{P}_i^T \underset{\sim}{R}(\underset{\sim}{U}_i + t \underset{\sim}{P}_i)$; however, past experience favors successive elastic solutions and this was done. Recent applications of the linear algorithm to 3D composite material problems by Dana[29] always converged to four places in less than N/5 cycles for problems of dimension N = 500 to over 2000. Applications in the present study have been to small one and two element models requiring N/2 cycles for similar accuracy.

Efficiency is also a function of the cost per cycle and this is where the vector processing efficiency of scientific computers helps iterative algorithms. Even the CDC 6600 can be made to compute dot products very efficiently by taking advantage of multiple arithmetic units. Unfortunately, older computers like the UNIVAC 1108 do not have this feature and because of their short 32 bit word, all arithmetic must be done in double precision. Several attempts to use mixed mode arithmetic on a UNIVAC 1108 were unsuccessful. The operation most sensitive to round-off error is the transformation of an element stiffness matrix from geometric format to point format. The reason is the large difference in the magnitude of displacements and displacement derivatives. Fortunately this can be avoided by transforming directly from algebraic format to point format. Another

factor affecting cycle efficiency is the amount of data transfer. In the present approach, only the reduced element matrices are transferred into core each cycle. Older versions of the program transferred the reduced structural matrix into core each cycle and this was more expensive primarily because the matrix had to be unpacked a few columns at a time. As a fringe benefit of using element matrices, the data transfer per cycle grows linearly with the number of elements in the model. The overall cycle cost then grows at most linearly since vector processing also increases at most linearly with the number of elements.

A constant issue in iterative methods is the convergence criteria. The first parameter to converge is the energy with the maximum modulus displacement component usually a close second. When these two parameters have converged to seven places, the stresses and strains have about three-place accuracy. Several additional cycles are required to produce stresses and strains that agree with the direct solution to six places (see Figure 6) and this raises the issue. Should these additional cycles be executed to increase the accuracy of the least significant stresses and strains and provide consistency with direct solutions? In linear problems this is done because the increase in cost is modest. However, in nonlinear problems, this expense is harder to justify since the intermediate solutions have no function other than to provide accurate state variables, like strain energy, so that accurate material properties can be computed.

## 4.0 APPLICATIONS

### 4.1 Carbon-Carbon Unit Cell

The processing of 3D carbon-carbon materials ideally results in an orthogonal array of fibers in which the open regions are filled with a carbon matrix material during densification. The repetitive volume element for the material has three planes of symmetry and Figure 7 shows schematically one octant of the so-called unit cell. Macroscopic properties for this material are usually based on an analysis of the unit cell with uniform traction or displacement boundary conditions as described by Ross[30]. A constant property finite element model of this composite would require a minimum of eight elements and the referenced analysis used twenty-seven elements. This same unit cell was modeled with only one variable property element using the techniques described earlier. The constituent properties for the fiber bundles and matrix material are given in Table 5 and a more complete description of the composite is given by Ross[30]. The results from the one element model are in remarkably good agreement with the results from other analyses presented in Table 6. There are several comments that need to be made about these results to maintain perspective: (1) the orthogonal nature of the weave allows the macroscopic properties to be computed from coarse models (2) the computer plot, Figure 8, of the free thermal expansion of the one element PATCHES-III model shows mesh lines at $\xi = L/6$ to enhance viewing and (3) imperfections in the unit cell can result in large differences between ideal and real material properties.

Given this perspective, one conclusion to be drawn is that without variable property modeling an analysis using the present element would cost over an order of magnitude more and not substantially change the mechanical properties. A second interesting conclusion is related to the poor estimate of $\alpha 11$ and the sensitivity of the macroscopic properties to constituent properties. The parametric cubic property modeling used $P(o) = P_o$, $P(1) = \dot{P}$, and $\dot{P}(o) = P(1) = 0$ boundary conditions which tend to lower the high modulus constituent data and raise the low modulus data. A sensitivity study revealed that $\alpha 11$ was primarily a function of the longitudinal

Table 5 Unit cell dimensions and constituent properties

L12 = 0.7, L13 = 0.3, L21 = 0.035, L23 = 0.015, L31= L32 = 0.0062

| | $Z_1^*$ | $Z_2^*, Z_3^*$ | Matrix |
|---|---|---|---|
| $E_L \times 10^{-6}$ | 33.34 | 4.841 | 0.70 |
| $E_T \times 10^{-6}$ | .8958 | 1.332 | 0.70 |
| $\nu_{LT}$ | .1818 | .1840 | 0.15 |
| $\nu_{TT}$ | .1898 | .1849 | 0.15 |
| $G_{LT} \times 10^{-6}$ | 1.169 | .9405 | 0.30435 |
| $G_{TT} \times 10^{-6}$ | .3765 | .5619 | 0.30435 |
| $\alpha_L \times 10^{6}$ | .5133 | 1.647 | 2.5 |
| $\alpha_T \times 10^{6}$ | .5149 | 4.571 | 2.5 |

*$Z_i$ Fiber bundle properties, reference 30.

Table 6 Unit cell macroscopic property comparisons

| | PATCHES-III (1-Element) | SAP* (27-Elements) | RULE-OF-MIXTURES |
|---|---|---|---|
| C11 x $10^{-6}$ | 11.793 | 12.461 | 12.460 |
| C12 x $10^{-6}$ | .274 | .226 | .230 |
| C13 x $10^{-6}$ | .248 | .214 | .222 |
| C22 x $10^{-6}$ | 2.274 | 2.328 | 2.340 |
| C23 x $10^{-6}$ | .251 | .211 | .225 |
| C33 x $10^{-6}$ | 1.518 | 1.376 | 1.416 |
| C44 x $10^{-6}$ | .846 | ------ | .853 |
| C55 x $10^{-6}$ | .760 | ------ | .754 |
| C66 x $10^{-6}$ | .625 | ------ | .609 |
| $\alpha$11 x $10^{6}$ | 1.462 | .748 | .755 |
| $\alpha$22 x $10^{6}$ | 2.896 | 2.567 | 2.271 |
| $\alpha$33 x $10^{6}$ | 4.284 | 3.924 | 4.039 |

*SAP results from reference 30.

$\alpha_L$ of the $Z_1$ fiber which is very small. In this case the parametric cubic model effectively doubled the $\alpha_L$ of the $Z_1$ and the boundary conditions for this property should be adjusted to give the correct area under the curve.

In addition to featuring the intra-element modeling capability, this application also raises the issue of sensitivity analyses. Schmit[31] has long advocated making analysis programs more design oriented by providing information on the sensitivity of the analysis results to design changes. The present formulation of the nonlinear material effects, Equation (16), allows such information to be computed by making the change in material properties constant with respect to a state variable and halting the iteration after the first or second cycle. This procedure was successfully applied to a unit cell analysis as part of another study.

4.2 Cracked Bar

To establish the utility of the parametrization in Table 3 for three-dimensional crack analyses, an internally cracked bar, Figure 9, studied by Gyekenyesi and Mendelson[32] was analyzed using a two element symmetry model. This problem is a finite dimensional version of the penny shaped or poker chip crack problem whose elasticity solution contains a square root strain singularity. The two element PATCHES-III model shown in Figure 10 uses parametrizations in the axial and radial directions that induce a square root strain singularity. When the singularity is at Z (1) rather than Z(o), as in the element over the crack face, the formal expression for Z ($\xi$) is

$$Z(\xi) = a\,(2\xi - \xi^2) \tag{21}$$

which lead to the same behavior at Z (1)

$$\begin{aligned} u_{,r} &= u_{,\xi}\,\xi_{,z}\,Z_{,r} \\ &= (a/2\sqrt{r})\,u_{,\xi} \end{aligned} \tag{22}$$

where $r = 1 - Z_1$ in this element and the comma notation indicates differentation. There are two features of the parametric cubic model that merit attention 1.) the geometry model is trivial to construct in algebraic or geometric format and

2.) the element displacement functions in geometric format have $u_{,\xi}(1)$ as a nodal variable which is directly related to the stress intensity factor. The coefficients for the algebraic, $S_i$, and geometric, $B_i$, representations of Equation (21) are simply

$$S_1 = 0,\ S_2 = -a,\ S_3 = 2a,\ S_4 = 0 \tag{23}$$

and

$$B_1 = 0,\ B_2 = a,\ B_3 = 2a,\ B_4 = 0 \tag{24}$$

The construction of the complete geometry model for this problem required six grid cards, two PATCHB directives containing only four nonzero $B_{ij}$ each, and two HPR directives. However, this easily constructed model is capable of accurately representing the highly deformed geometry, Figure 11, as the crack opens under an axial load.

Comparison between the present solution and the Gyekenyesi-Mendelson solution, Figure 12, show good stress agreement. The strains in PATCHES-III are computed at the Gaussian points and then transformed to the one-third points which accounts for the finite amplitude stresses at r = 0. The stress intensity factor computed from $u_{,\xi}(1)$ of the element containing the crack face is 2.5% higher than that for an infinite dimension bar whch is slightly closer than the Gyekenyesi-Mendelson result. The displacements are also correspondingly closer to classical than theirs. The parametric derivative $u_{,\xi}$ in the present model may provide a convenient characterization of stress intensity. The issue would depend on its behavior under admissible reparametrizations such as those in Table 2. Since in general the strength of the singularity is unknown and changes as a function of material anisotropy[33]. A carpet plot of the radial strain component over the $(Z_1, Z_3)$ plane, Figure 13, shows a theta dependence in keeping with the elasticity solution which contains sin $\theta$ and cos $\theta$ terms in the strains.

4.3 Graphite Bar

Consider next the application of a stress-strain state variable model to a composite material whose inelastic behavior is known to differ significantly from that

of metals. ATJ-S graphite is one such material and its inelastic behavior has been extensively tested by Jortner[2] in biaxial and triaxial stress states. To focus clearly on the ability of the model to represent inelastic behavior not normally found in metals, a case of hydrostatic compression was selected. A classical plasticity solution would be identical to the elasticity solution for hydrostatic loading. This material, however, is quite nonlinear under hydrostatic compression and the Batdorf model for ATJ-S fits the Jornter test data extremely well, Figure 14. A transversely isotropic graphite bar, diameter 0.250 inches by 4.0 inches was loaded by an axial force and external pressure in these tests. The stress-strain version of the Batdorf model was used to compute the data in Figure 14 assuming constant strain ratios which is consistent with the Jortner results. The bar elastic constants and $F_{ijkl}$ for the Batdorf model are given in Table 7 where the across grain direction coincides with the centerline of the bar and the $\sigma^o$ parameters are $\sigma_r^o = \sigma_\theta^o$ and $\sigma_z^o$ in,

$$V_2 = C^o \left\{ \left[ \left( \frac{\sigma_z}{\sigma_z{}^0} \right)^2 + \left( \frac{\sigma_\theta}{\sigma_\theta{}^0} \right)^2 + \left( \frac{\sigma_r}{\sigma_r{}^0} \right)^2 + 2 \left( \frac{\sigma_{z\theta}{}^2}{\sigma_z{}^0 \sigma_\theta{}^0} + \frac{\sigma_{zr}{}^2}{\sigma_z{}^0 \sigma_r{}^0} + \frac{\sigma_{r\theta}{}^2}{\sigma_r{}^0 \sigma_\theta{}^0} \right) \right]^{1/2} - 1 \right\} \quad (25)$$

These constants are determined from unaxial data including the constant multiplier, $C^o$, where $C^o = 0.15$ for ATJ-S. The use of constant strain ratios in the axial tension range causes the stress ratios from the Batdorf model to deviate slightly from $\pm 1$ but this difference is small even up to $\varepsilon_z = 0.004$ as Figure 14 demonstrates.

Table 7 Graphite bar material constants

| DIRECTION | E | $\nu$ | G | $\sigma^o$ |
|---|---|---|---|---|
| With Grain (r, $\theta$) | $1.8 \times 10^6$ | 0.1 | $0.8 \times 10^6$ | $1.22 \times 10^3$ |
| Across Grain (z) | $1.2 \times 10^6$ | 0.1 | $0.65 \times 10^6$ | $1.04 \times 10^3$ |

A PATCHES-III model of the gage section of the test specimen was developed using the material constants from Table 7. The geometric simplicity and transverse isotropy allowed a simple one element symmetry model of a $30^{o}$ segment of the bar to be used. A single hydrostatic load condition of 4 ksi compression was analyzed using successive elastic solutions of Equation (15) starting from the linear solution. Convergence of the pseudo-force method was rapid as Figure 15 illustrates and the resulting strains are in good agreement, Figures 16 and 17, with Jortner's test data. In this particular problem the exact stress solution is known from equilibrium considerations and the iteration was terminated when the stresses were within one percent of the exact solution. The convergence characteristics of several interesting parameters are shown in Table 8.

Table 8 Nonlinear solution convergence data

| Cyle | $\sigma$ | Potential Energy | $V_2$ | $Q_{max}$ |
|---|---|---|---|---|
| 0 | -4000 | -.00614 | .7537 | 0.0 |
| 1 | -3748 | -.00973 | .5189 | 2.33 |
| 2 | -3845 | -.00119 | .6335 | 3.52 |
| 3 | -3909 | -.00132 | .6882 | 4.17 |
| 4 | -3948 | -.00139 | .7171 | 4.54 |
| 5 | -3970 | -.00143 | .7331 | 4.75 |
| $\infty$ | -4000 | ------- | .7337 | ----- |

The computational performance of the model on an UNIVAC 1108 was good, taking less than one minute per pseudo-load cycle for this small problem and should be better on a parallel processing machine. The number of conjugate gradient cycles required to maintain constant solution accuracy decreased with each pseudo-load cycle but not dramatically. The original linear solution starting from zero used 74 cycles and the last solution required 54 cycles. The time required to generate $Q_n$ each cycle was negligible in comparison to the matrix solution costs.

## 5.0 CONCLUSIONS

The computational system designed and developed in this study has the flexibility to encompass most of the available inelastic composite material models and appears to have the efficiency to make its use feasible if not practical. It will require additional experience and testing in a variety of applications before the efficiency of the system can be fully established but the basic design philosophy seems sound; namely, better computers are a more likely development than better numerical methods. The use of stress or strain state variable modeling is certainly not new but the design of one standard input format for a entire class of material models is a step forward.

The introduction of isoparametric modeling for material properties as well as geometry is another important step required by the variability of composite materials. In each instance mentioned, the results presented are a beginning with much additional work required before the triaxial inelastic behavior of composites is encompassed by the available models. This work should include:

1. Multiaxial testing programs, such as Jortners, for other three-dimensional composites that includes a parallel computational model development effort.

2. Extensions to include interstitial slip with friction at bimaterial interfaces. This behavior in fiber reinforced composites is important to an understanding of microstructural effects on the failure of these materials.

3. Development of alternatives to point stresses and strains as a measure of composite material response for structural applications.

4. Development of representative volume element models suitable for inelastic behavior and failure that account for the statistical nature of three-dimensional composites.

## REFERENCES


1. Drucker, D. C., "Yielding, Flow and Failure," in Inelastic Behavior of Composite Materials edited by C. T. Herakovich, AMD Vol. 13, 1975.

2. Jortner, J., "Multiaxial Response of ATJ-S Graphite," AFML-TR-73-170, October, 1973.

3. Batdorf, S. B., "A Polyaxial Stress-Strain Law for ATJS Graphite," Journal of the American Ceramic Society, Vol. 59, 1976, pp. 308-312.

4. Jones, R. M. and Nelson, D. A. R., Jr., "A New Material Model for the Nonlinear Biaxial Behavior of ATJ-S Graphite," Journal of Composite Materials, Vol. 9, 1975, pp. 10-27.

5. Liu, T. C., Nilson, A. H. and Slate, F. O., "Stress-Strain Response and Fracture of Concrete in Uniaxial and Biaxial Compression," American Concrete Institute Journal, May, 1972, pp. 291-295.

6. Francis, P. H. and Bert, C. W., "Composite Material Mechanics: Inelasticity and Failure," Fibre Science and Technology, Vol. 8, 1975, pp. 1-19.

7. Saczalski, K. J. and Stricklin, J. A., eds., "The Office of Naval Research Plasticity Workshop," Texas A & M University Report 75-51, June, 1975.

8. Lin, T. H. and Ito, M., "Theoretical Plastic Stress-Strain Relationship of a Polycrystal and the Comparisons with the Von Mises and the Tresca Plasticity Theories," International Journal of Engineering Science, Vol. 4, 1966.

9. Havner, K. S. and Varadarajan, R., "A Quantitative Study of a Crystalline Aggregate Model," International Journal of Solids and Structures, Vol. 9, 1973, pp. 379-394.

10. Esterling, D. J., "Computer Simulation of Screw Dislocation in Aluminum," Proceedings of the 13th Annual Society of Engineering Science Meeting, NASA CP-2001, Vol. 1, 1976, pp. 137-146.

11. Stricklin, J. A., Haisler, W. E. and Von Rieseman, W. A., "Nonlinear Continua," in Structural Mechanics Computer Programs, University Press of Virginia, 1974, pp. 3-36.

12. Barsoum, R. S. and Loomis, R. W., "Inelastic Finite Element Cyclic Analysis of a Nozzle-to-Cylinder Intersection," ASME Paper No. 76-PVP-29, 1976.

13. Stanton, E. L., Crain, L. M. and Neu, T. F., "A Paremetric Cubic Modeling System for General Solids of Composite Material," International Journal for Numerical Methods in Engineering, Vol. 11, 1977, pp. 653-670.

14. Buch, J. D., "Mechanical Behavior Model for Graphites," in Properties Related to Fracture Toughness, ASTM STP-605, 1976, pp. 124-144.

15. Nueber, H., "Anisotropic Nonlinear Stress-Strain Laws and Yield Conditions," International Journal of Solids and Structures, Vol. 5, 1969, pp. 1299-1310.

16. Weiler, F. C., "DOASIS, A Computer Program for the Deformation Plastic, Orthotropic, Axisymmetric (and Plane) Solution of Inelastic Solids," AFML-TR-75-37, Vol. 1, 1975.

17. Chung, T. J., "Thermomechanical Response of Inelastic Fibre Composites," International Journal for Numerical Methods in Engineering, Vol. 9, 1975, pp. 169-185.

18. Valliappan, S., Boonlualohr, P., and Lee, I. K., "Nonlinear Analysis for Anisotropic Materials," International Journal for Numerical Methods in Engineering, Vol. 10, 1976, pp. 597-606.

19. Rybicki, E. F., "An Incremental Complementary Energy Method of Nonlinear Stress Analysis," Ph.D. Thesis, Case Institute of Technology, 1968, pp. 17-21.

20. Hahn, H. T. and Tsai, S. W., "Nonlinear Elastic Behavior of Unidirectional Composite Laminae," Journal of Composite Materials, Vol. 7, 1973, pp. 102-118.

21. Jones, R. M. and Morgan, H. S., "Analysis of Nonlinear Stress-Strain Behavior of Fiber-Reinforced Composite Materials," in Proceedings AIAA/ASME/SAE 17th SDM Conference, 1976, pp. 174-183.

22. Henshell, R. D. and Shaw, K. G., "Crack Tip Elements are Unnecessary," International Journal of Numerical Methods in Engineering, Vol. 9, 1975, pp. 495-507.

24. Coons, S. A., "Surfaces for Computer Aided Design of Space Forms," M.I.T. Report No. MAC-TR-41, 1967.

25. Lossing, D. L. and Eshleman, A. L., "Planning a Common Data Base for Engineering and Manufacturing," Douglas Aircraft Paper No. 6300, presented to SHARE XLIII, 1974.

26. Havner, K. S., "On Convergence of Iterative Methods in Plastic Strain Analysis," International Journal of Solids and Structures, Vol. 4, 1968, pp. 491-508.

27. Stricklin, J. A., Hailsler, W. E. and Von Riesemann, W. A., "Evaluation of Solution Procedures for Material and/or Geometrically Nonlinear Structural Analysis," AIAA Journal, Vol. 11, 1973, pp. 292-299.

28. Fox, R. L. and Stanton, E. L., "Developments in Structural Analysis by Direct Energy Minimization," AIAA Journal, Vol. 6, 1968, pp. 1036-1042.

29. Dana, J., "Three-Dimensional Finite Element Analysis of Thick Laminated Composites," Ph.D. Thesis, Virginia Polytechnic Institute, 1974, Chapter III-C.

30. Ross, A. L., "Designing Three-Directional Composites," ASME Mechanical Engineering, 1975, pp. 32-37.

31. Schmit, L. A., Jr., "The Structural Synthesis Concept and its Potential Role in Design with Composites," in Proceedings of the Fifth Symposium on Naval Structural Mechanics, Mechanics of Composite Materials, Pergamon Press, 1970, pp. 553-582.

32. Gyekenyesi, J. P. and Mendelson, A., "Three-Dimensional Elastic Stress and Displacement Analysis of Finite Geometry Solids Containing Cracks," NASA TM X-71467, 1974.

33. Erdogan, F. and Delale, F., "On the Problem of Stress Singularities in Bonded Orthotropic Materials," in Proceedings of the 13th Annual Meeting of the Society of Engineering Science, NASA CP-2001, Vol. 1, 1976, pp. 291-300.

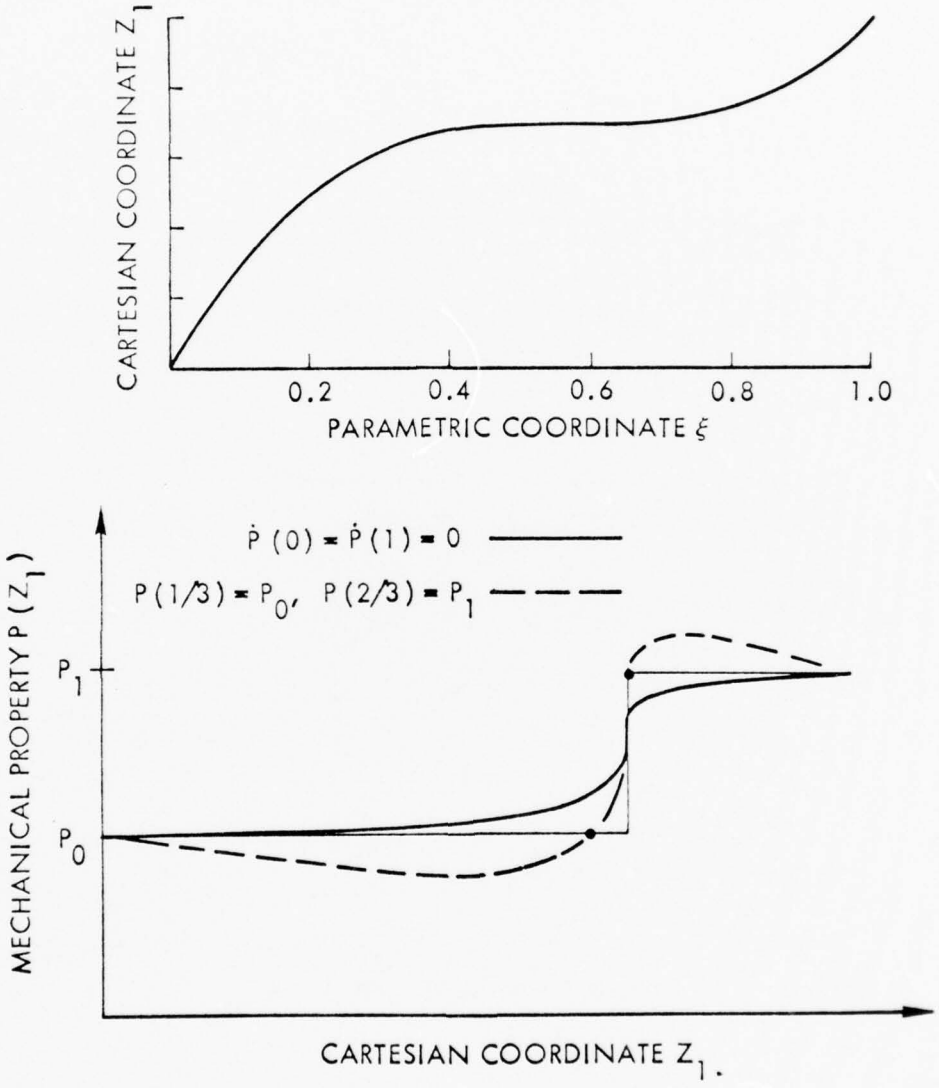


Figure 1. Parametric Cubic Modeling of a Bimaterial Interface

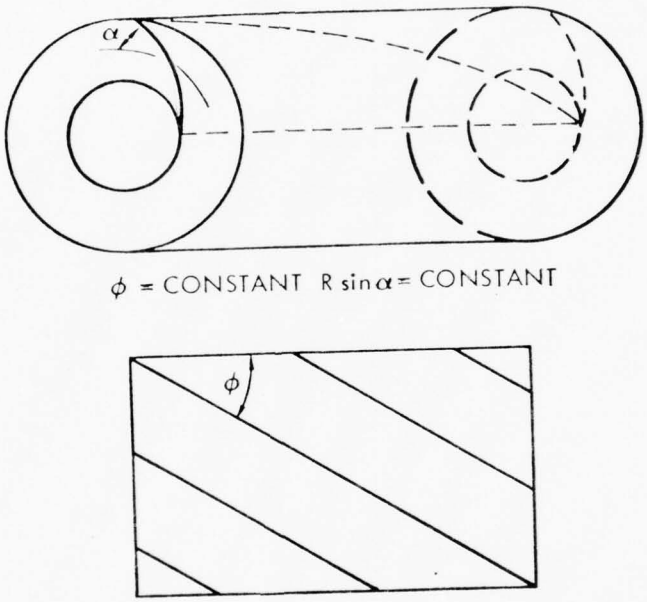


Figure 2. Rosette Construction Materials

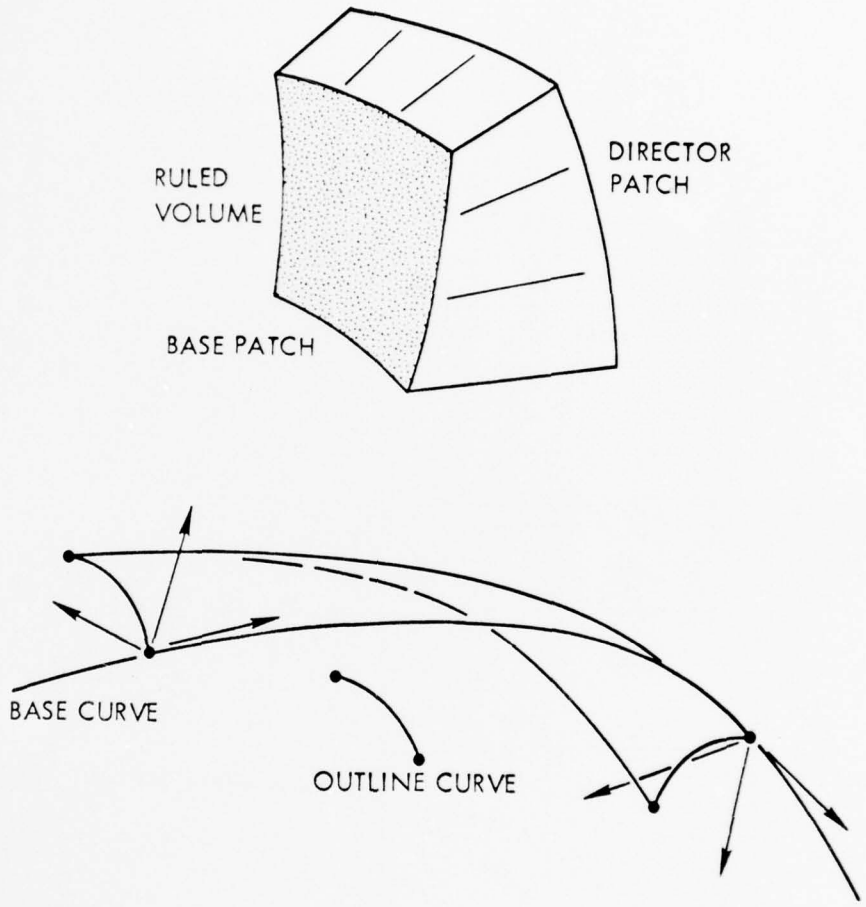


Figure 3. Construction of Finite Geometry Models

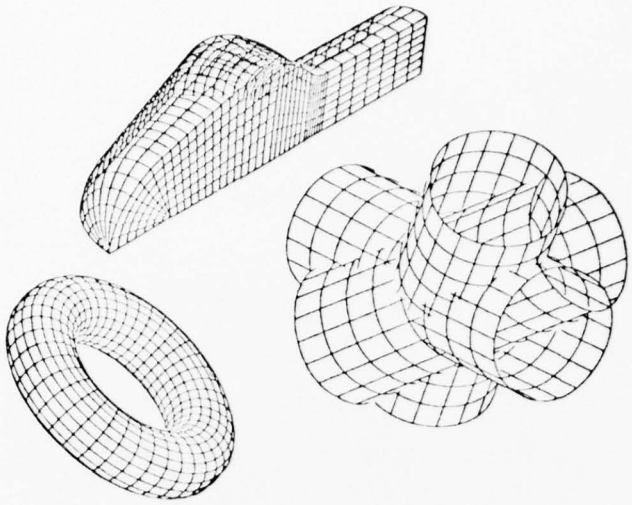

Figure 4. Parametric Cubic Models

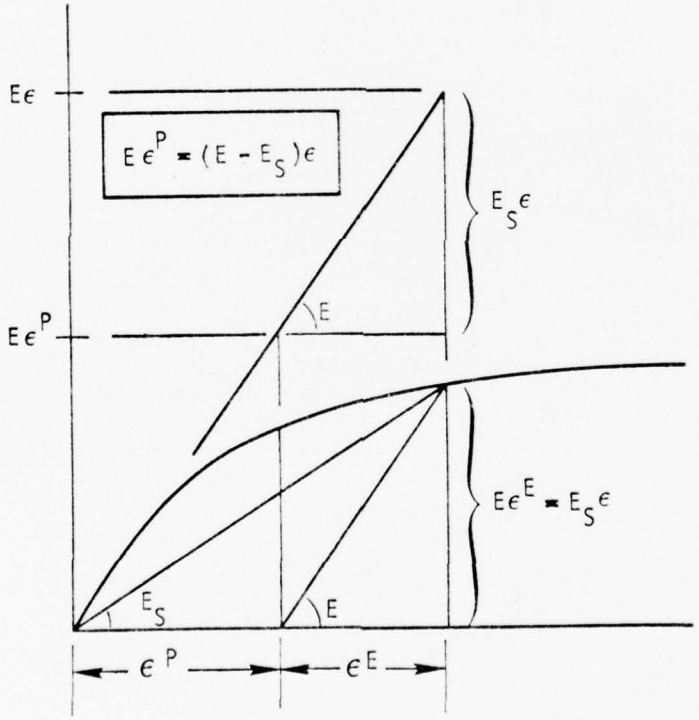


Figure 5. Stress-strain Schematic

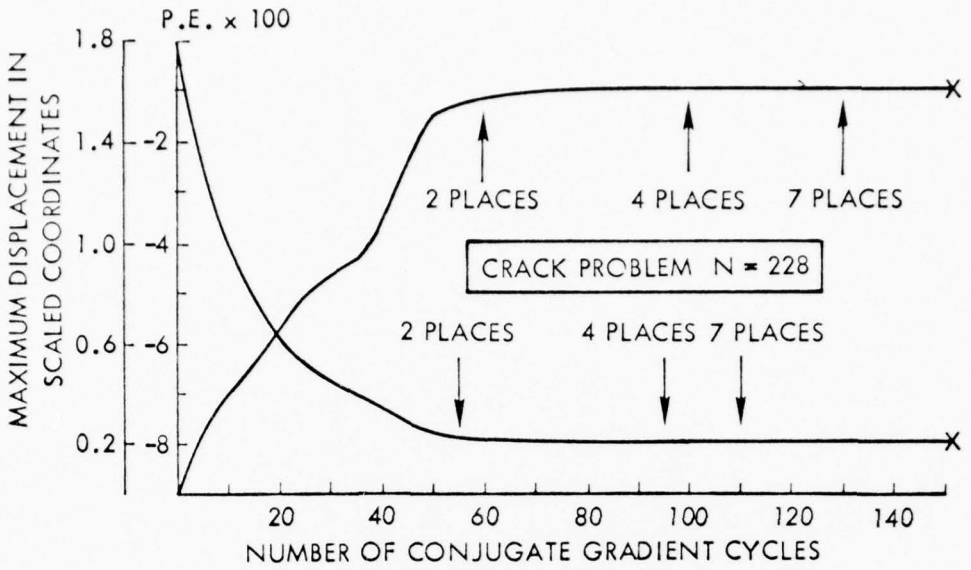


Figure 6. Energy Convergence of the Conjugate Gradient Solution

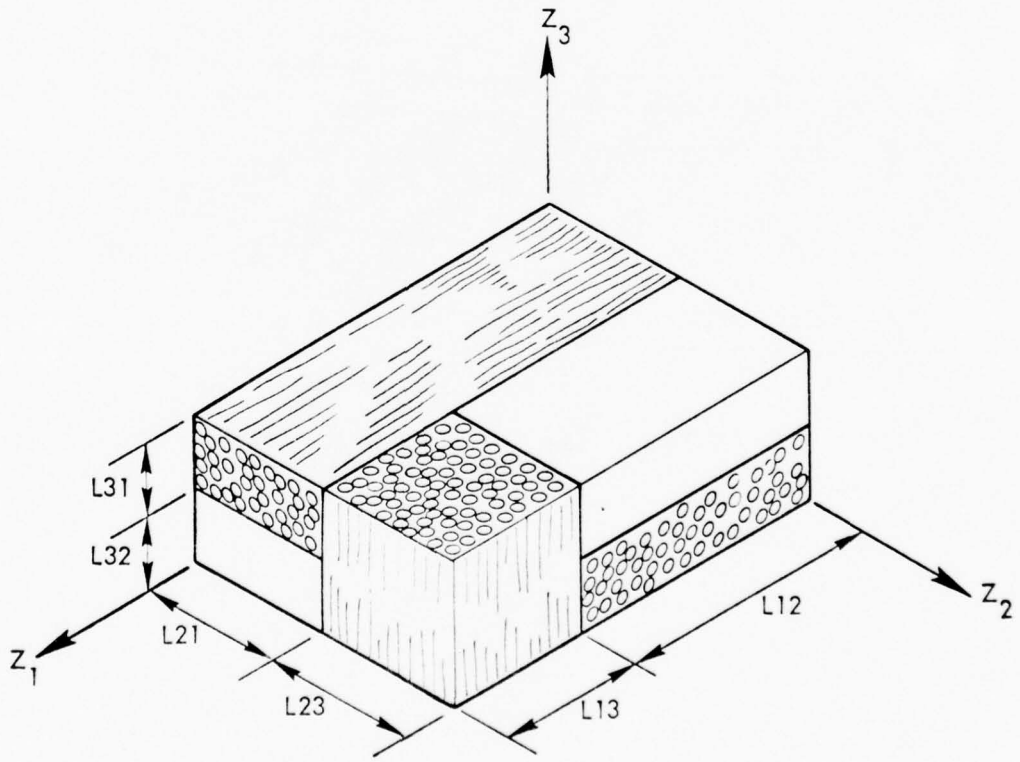


Figure 7. Carbon-carbon Unit cell Schematic



BULK DATA DECK

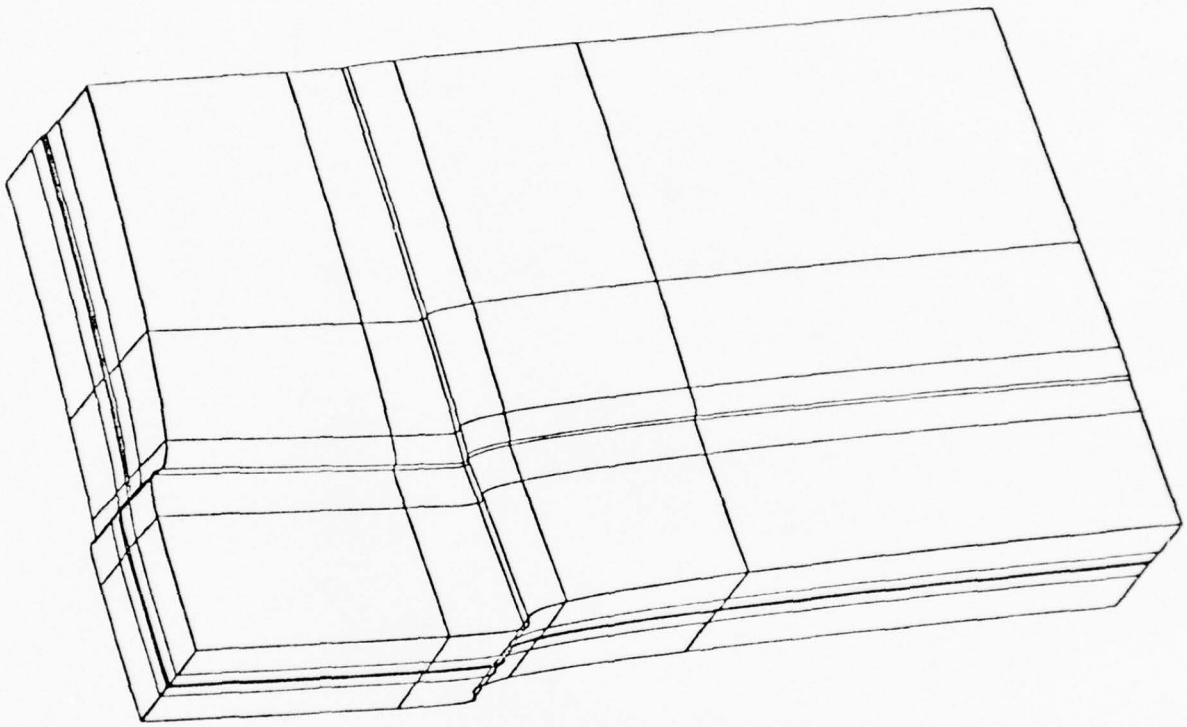

Figure 8. Unit Cell Thermal Expansions

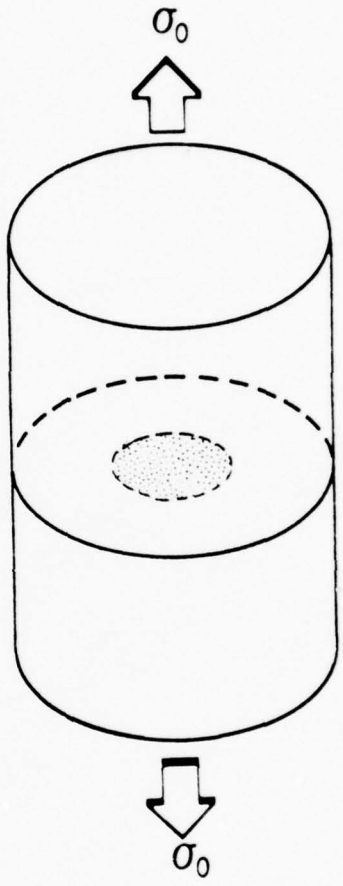


Figure 9. Cracked Bar Schematic

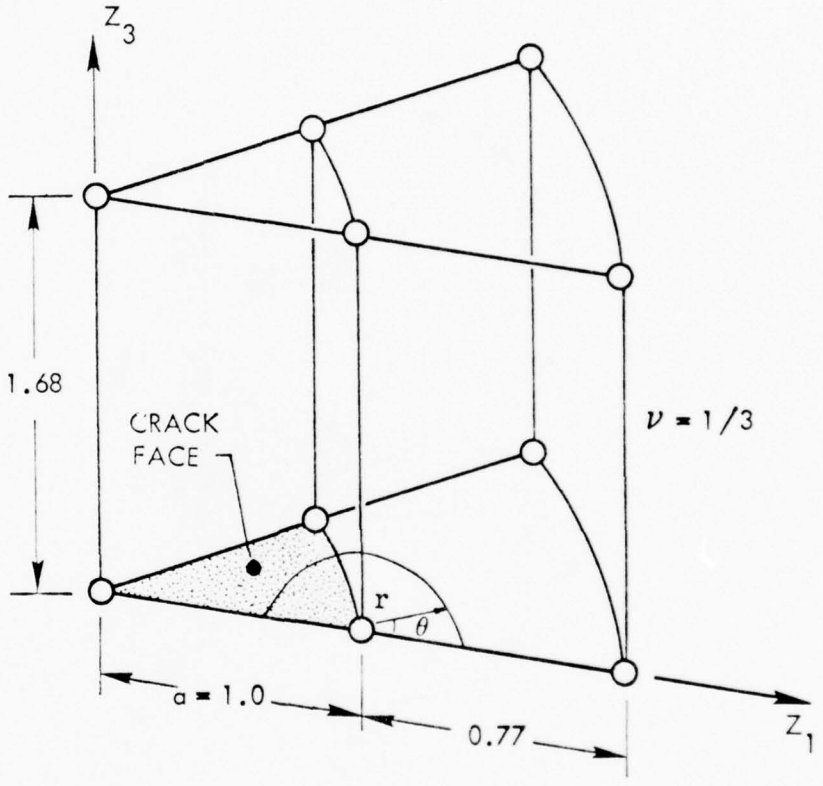


Figure 10. PATCHES-III Model of Cracked Bar

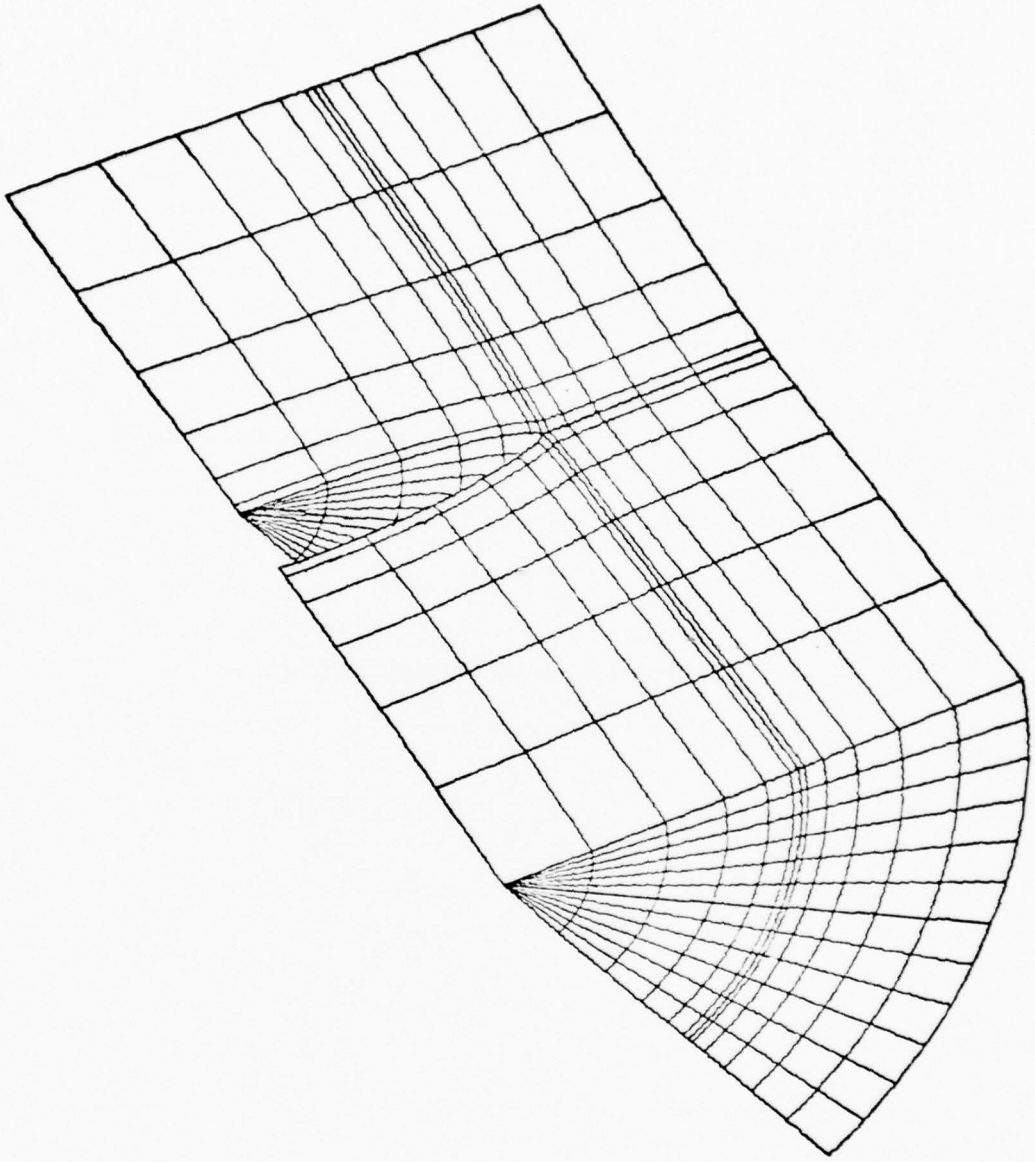

Figure 11. Cracked Bar Elastic Deformations

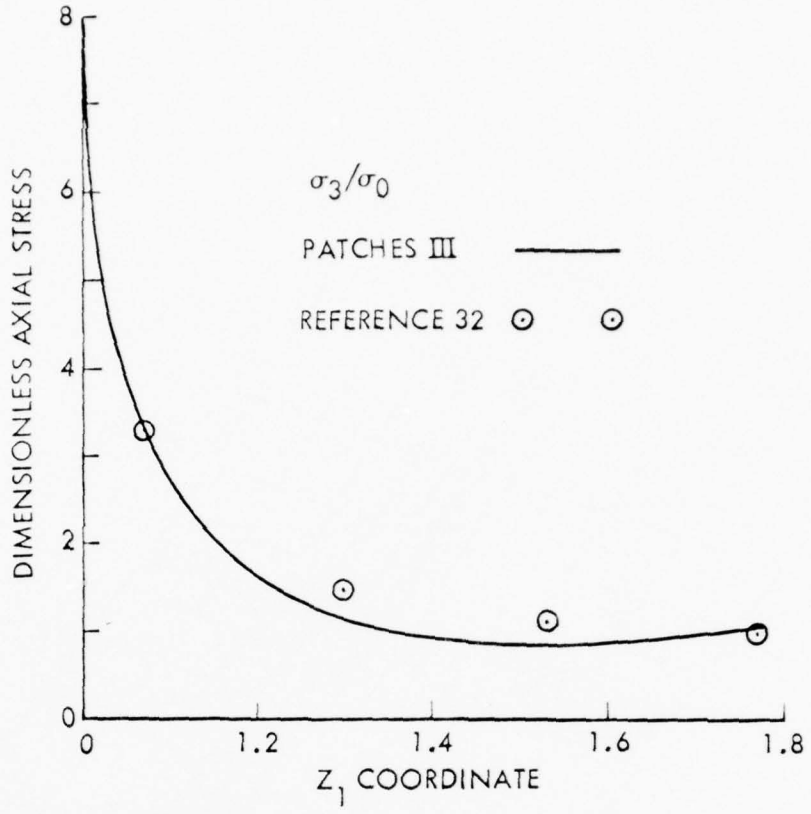


Figure 12. Cracked Bar Axial Stress Comparisons

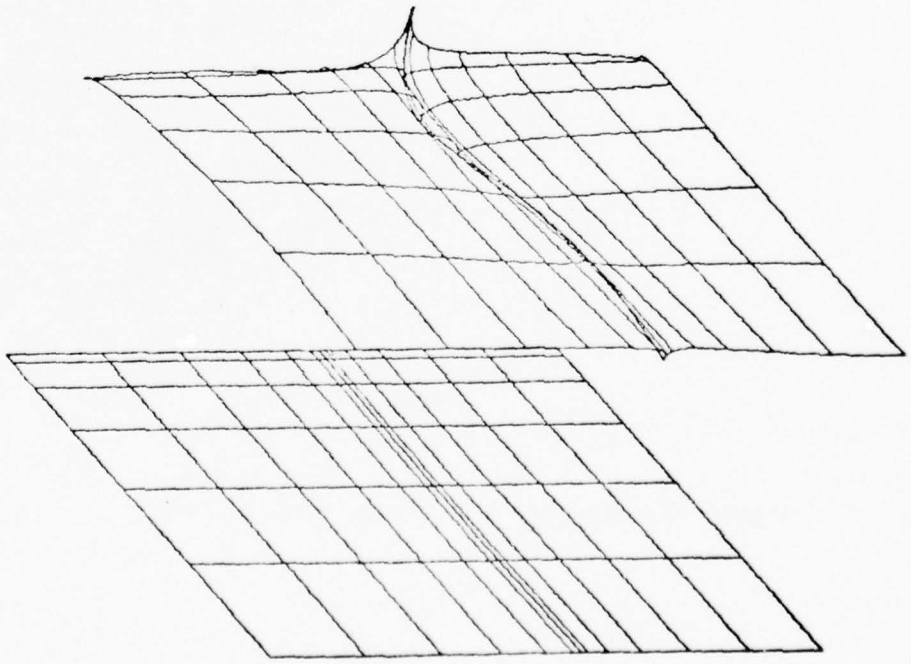

Figure 13. Cracked Bar Radial Strain Display

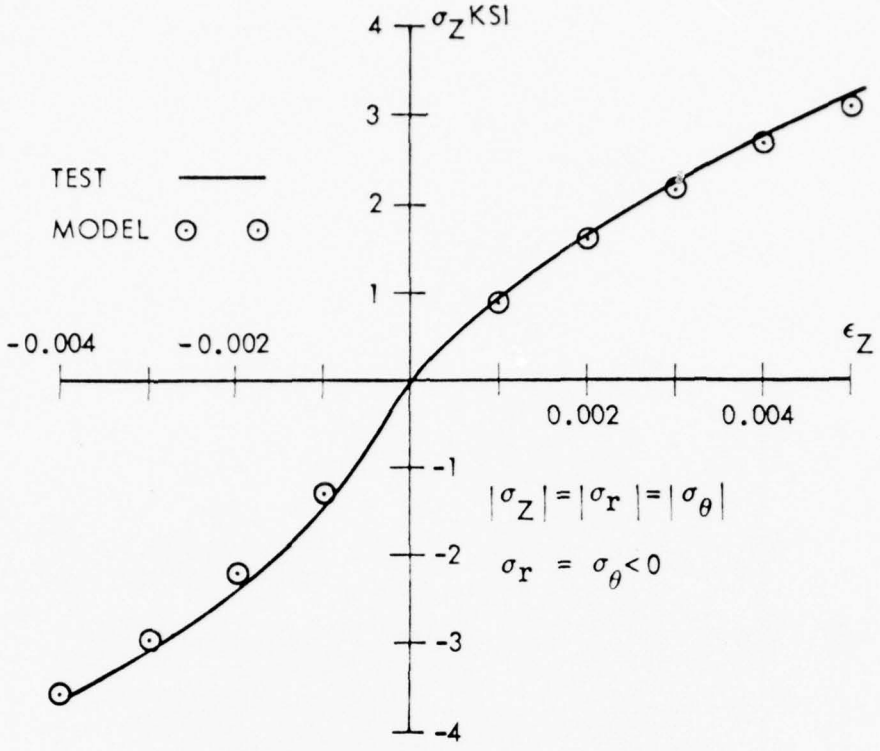


Figure 14. ATJ-S Triaxial Stress-Strain Comparisons

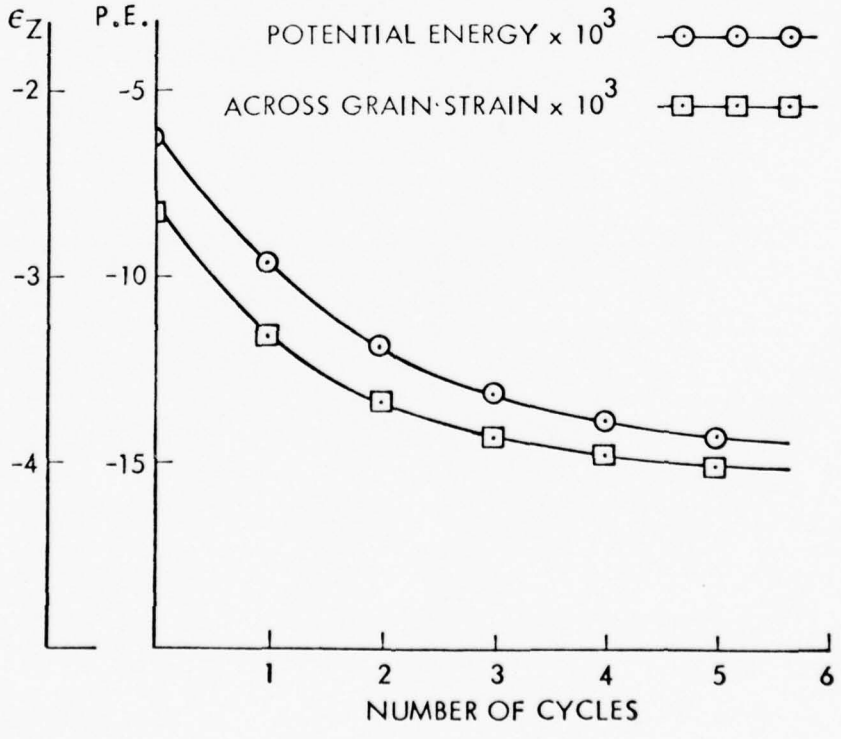


Figure 15. Convergence of Pseudo-force Method

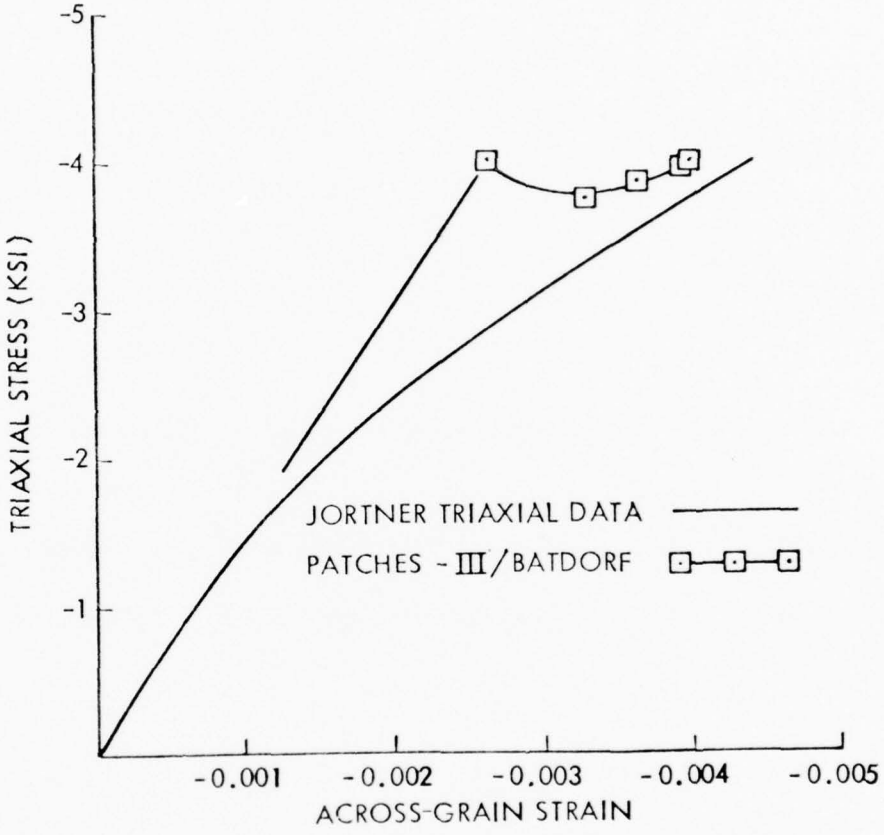


Figure 16. Inelastic Across-grain Strain Convergence

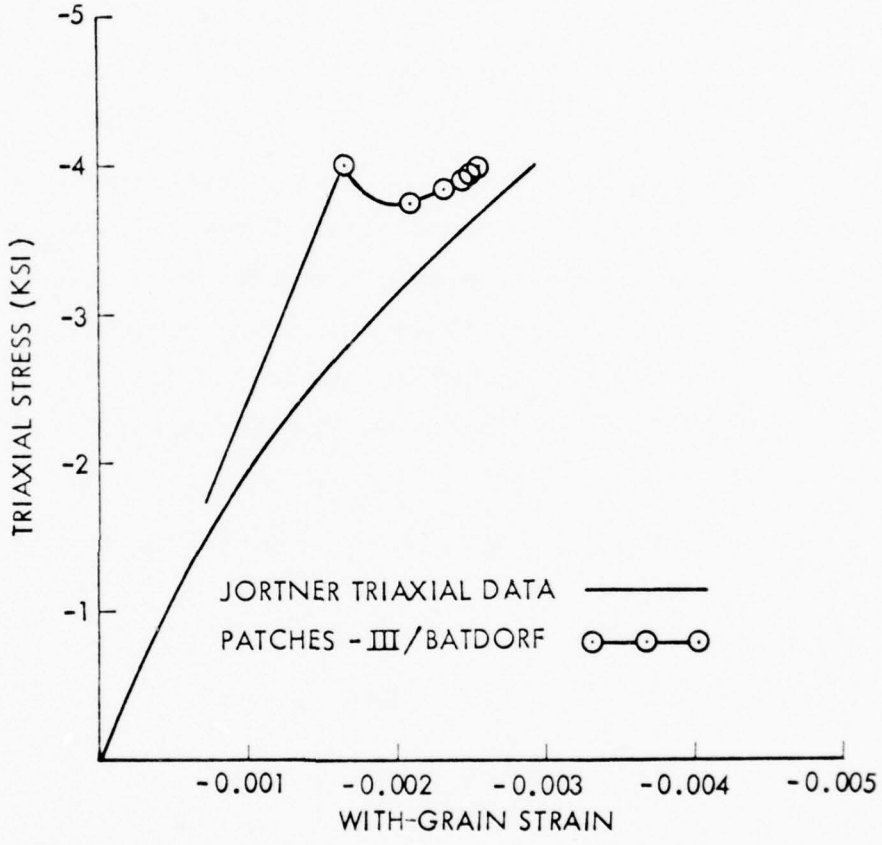


Figure 17. Inelastic With-grain Strain Convergence

# APPENDIX

The program updates for nonlinear material modeling in PATCHES-III were made using the generalized postprocessor system GPOSTP. This system interfaces with PATCHES-III through three files: PPDATA, INPT and RANDOM16 created during a normal execution of a linear elastic analysis. Any routine in the PATCHES-III library is available to GPOSTP and allows new capability, like MATN, to be fully developed and tested before restructuring the original code.

In the present effort a major change had to be made to the code to cope with large nonlinear matrix problems. These changes are complete and the restructured code is shown in the update to Figure 4-2 of the programmers manual. The GPOSTP system for the MATN postprocessor is shown in Figure 4-2a. The limited testing of MATN accomplished during the study has been very successful. This link will be added to the basic system after all options are fully tested.

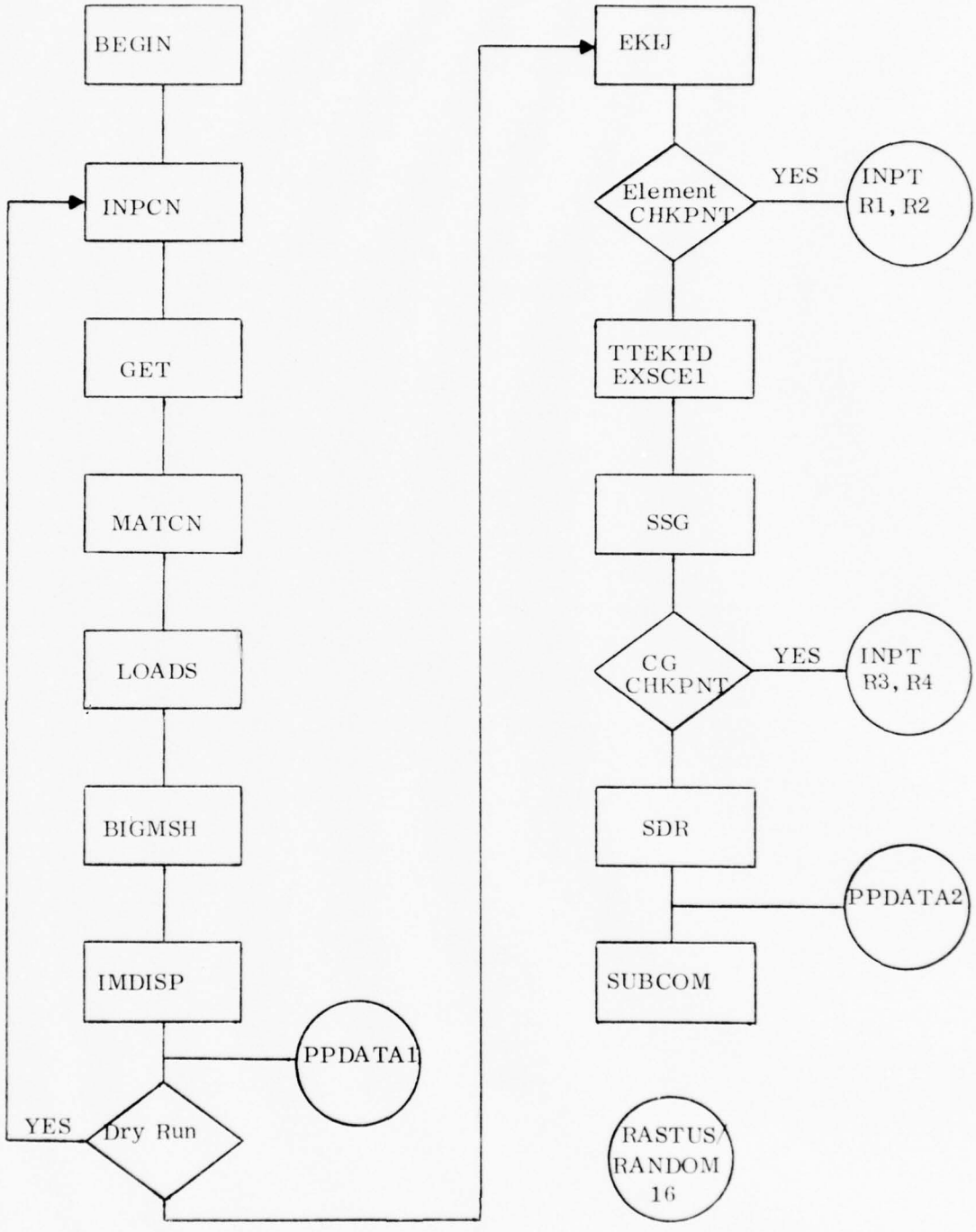


Figure 4-2. Basic Flow PATCHES-III Version 7

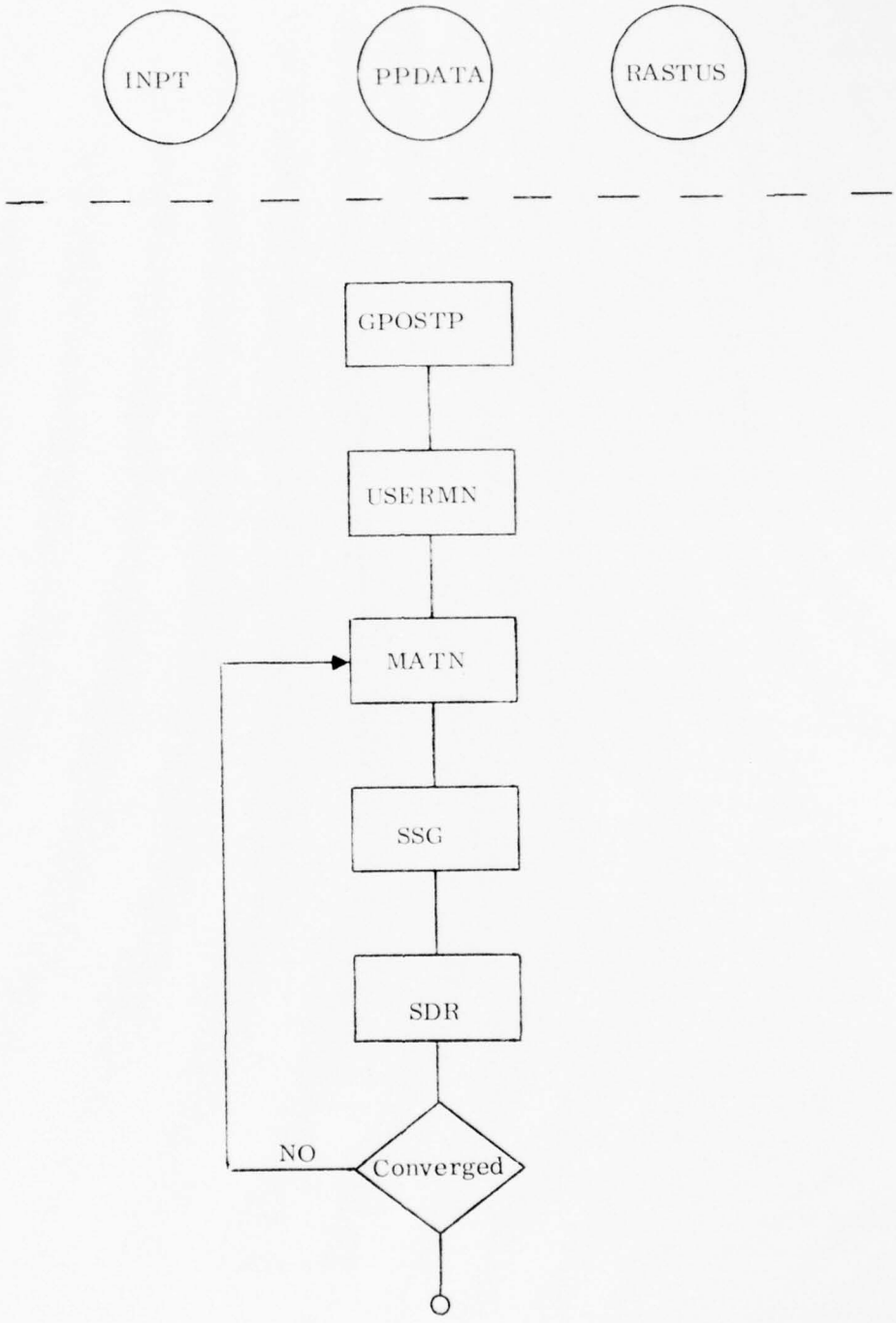


Figure 4-2a. Basic Flow MATN Postprocessor

Input Data Card: PATCHGR Patch generated by general line rotation.

Description: Generates a bicubic patch for the surface created by rotating a PC line about a general axis of rotation through gamma degrees.

Format and Example:

| 1 | 2 | 3 | 4 | 5 | 6 | 7 | 8 | 9 | 10 |
|---|---|---|---|---|---|---|---|---|---|
| PATCHGR | ID | LID, SEG | ZA1 | ZA2 | ZA3 | ZB1 | ZB2 | ZB3 | +P1 |
| PATCHGR | 5 | 3 | 1.5 | 0. | -3.0 | | 2.5 | 0.3 | +P1 |
| +P1 | TID | GAMMA | GAMMAO | | | | | | |
| +P1 | | 25 | | | | | | | |

| Field | Contents |
|---|---|
| ID | The identification number to be given the patch generated from line LID, segment number SEG. |
| LID, SEG | The line number, LID, and segment number, SEG, that identifies the PC line to be rotated. A blank SEG defaults to one. |
| ZAI, ZBI | Coordinates of two points that define the rotation axis directed from $\underset{\sim}{Z}_A$ to $\underset{\sim}{Z}_B$. |
| TID | Transformation ID, if any, that defines a geometric transformation to be applied to the PC line before rotation. The line, LID, does not change. |
| GAMMA, | The angle in degrees through which the PC line is rotated starting $\gamma_o$ degrees from the initial position of the line. The sense of rotation is determined by the right-hand rule and the directed line (vector) from $\underset{\sim}{Z}_A$ to $\underset{\sim}{Z}_B$. |

Input Data Card: PATCHO Outline patch(es)

Description: The patch(es) generated by moving an outline curve along a base curve with a fixed orientation of the outline curve in the global frame or in the local Frenet frame of the base.

Format and Example:

| 1 | 2 | 3 | 4 | 5 | 6 | 7 | 8 | 9 | 10 |
|---|---|---|---|---|---|---|---|---|---|
| PATCHO | ID1 | BLID, SEG | OLID, SEG | TID | FRAME | ID2 | ... | IDN | |
| PATCHO | 5 | 6,1 | 3 | | F | 11 | THRU | 15 | |

| Field | Contents |
|---|---|
| ID1 | Patch identification number for first patch generated. |
| BLID, SEG | Baseline identification number, and segment number, SEG. If the SEG is not specified, the entire line BLID is used. |
| OLID, SEG | Outline curve identification number, and segment number, SEG. If the SEG is not specified, the entire line OLID is used. |
| TID | Transformation ID, if any, that defines a rotation matrix to reorient the outline curve relative to the base curve. The outline curve is always translated to the first grid point of the baseline independent of TID. |
| FRAME | E for fixed outline orientation with respect to the Cartesian frame. F for fixed outline orientation with respect to the local Frenet frame of the base curve. |
| ID2, 3, .., N | List of identification numbers to be given the second and subsequent patches generated, if any. This sequence proceeds from the second line segment of OLID to last and then repeats from the first segment for the next segment of BLID. |

Input Data Card: MATOR Orthotropic Material Definition

Description: Defines the material properties for a linear, temperature independent, orthotropic material from engineering constants

Format and Example:

| 1 | 2 | 3 | 4 | 5 | 6 | 7 | 8 | 9 | 10 |
|---|---|---|---|---|---|---|---|---|---|
| MATOR | MID | FRAME | POINTS | O1 | O2 | .. | ON | | |
| MATOR | 3 | 1 | 8 | 2 | 6 | THRU | 12 | | |

| Field | Contents |
|---|---|
| MID | Material identification number |
| FRAME | =1, Properties are in an orthonormal Cartesian frame<br>=2, Properties are in the normalized parametric frame of the element. Assumes parametric frame is quasi cylindrical or speherical. |
| POINTS | =1, Constant material properties (N=1).<br>=8, Trilinear variation of material properties (N=8).<br>=64, Tricubic variation of material properties (N=1). |
| O1,O2, . . ,ON | Matrix identification number for the orthotropic material engineering constants at the interpolation points. If POINTS is equal 64 a single entry is used to identify a matrix containing the 64 OID's. |

Remarks:

1. The engineering constants are entered in sequence $E_{11}$, $E_{22}$, $E_{33}$, $\upsilon_{12}$, $\upsilon_{13}$, $\upsilon_{23}$, $G_{12}$, $G_{13}$, $G_{23}$ on the MTRX matrix card (s).

2. The Air Force Design Guide convention for Poisson ratios is used i.e. $E_{ii}\,\upsilon_{ji} = E_{jj}\,\upsilon_{ij}$.

BULK DATA DECK

Input Data Card: MATN Nonlinear Material Properties.

Description: Defines the nonlinear behavior of a material property in terms of stress or strain state variables.

Format and Example:

| 1 | 2 | 3 | 4 | 5 | 6 | 7 | 8 | 9 | 10 |
|---|---|---|---|---|---|---|---|---|---|
| MATN | MID | MPID | MAT | SHAPE | STATE1 | STATE2 | | | +M1 |
| MATN | 10 | | MATO | CC | V2 | | | | +M1 |
| +M1 | TI | MTRX-M | V1 | MTRX-V1 | V2 | MTRX-V2 | | | +M2 |
| +M1 | 500. | 6 | 100.0 | 6 | | | | | +M3 |

| Field | Contents |
|---|---|
| MID | Material identification number. |
| MPID | Identification number of the matrix that defines the mesh points which have these properties. The default is all mesh points in an element. |
| MAT | Mnemonic that defines the format of the data in MTRX-M. |
| SHAPE | Mnemonic that defines the interpolation method for T, V1, V2 in that order; CLL, LCC, etc. where L = Linear and C = Cubic. |
| STATEI | Mnemonic that identifies state variable I (see remarks). |
| VI | Value of the variable I for which these data apply. A blank field requires MTRX-VI data to define VI. |
| TI | Temperature at which these data apply. The default is all temperatures. |
| MATRX-M | Matrix identification number of properties data in the format defined by MAT. |
| MTRX-VI | Matrix identification number of coefficients that define VI. |

Remarks

1. The standard state variables are VI and VBI for I = 1, 2, 3, 4 where V1 = $F_i \epsilon_i$, VB4 = $F_{ijkl}\, \sigma_i \sigma_j \sigma_k \sigma_1$, etc.
2. The only non-standard options are the Batdorf model identified by a B and the Lee identified by an L.

Input Data Card: TMOVE Rigid Body Transformation

Description: Defines a transformation that move objects (lines, patches, hyper-patches) as rigid bodies.

Format and Example:

| 1 | 2 | 3 | 4 | 5 | 6 | 7 | 8 | 9 | 10 |
|---|---|---|---|---|---|---|---|---|---|
| TMOVE | ID | Z01 | Z02 | Z03 | DCID | Ψ | θ | Φ | +TA |
| TMOVE | 1 | 3.0 | 0. | 3. | | 30. | 20. | -10. | +TA |
| +TA | T1 | T2 | T3 | | | | | | |
| +TA | 3.0 | 0. | 4.0 | | | | | | |

Field — Contents

ID — Transformation identification number (1 to 100).

ZOI — Defines an origin for rotation of the object.

DCID — Direction cosine matrix identification number. If blank or zero, the Euler angles Ψ, θ, Φ, define the rotation matrix.

Ψ, θ, Φ — Euler angles in the 3, 1, 3 rotation sequence.

$$R = \begin{pmatrix} \cos\psi\cos\phi - \cos\theta\sin\phi\sin\psi & -\sin\psi\cos\phi - \cos\theta\sin\phi\cos\psi & \sin\theta\sin\phi \\ \cos\psi\sin\phi + \cos\theta\cos\phi\sin\psi & -\sin\psi\sin\phi + \cos\theta\cos\phi\cos\psi & -\sin\theta\cos\phi \\ \sin\theta\sin\psi & \sin\theta\cos\psi & \cos\theta \end{pmatrix}$$

TI — Defines a translation to be applied after the rotation.

Remarks:

1. The complete transformation can be defined as

$$\underset{\sim}{Z}^* = R\,(\underset{\sim}{Z} - \underset{\sim}{Z}_O) + \underset{\sim}{T}$$

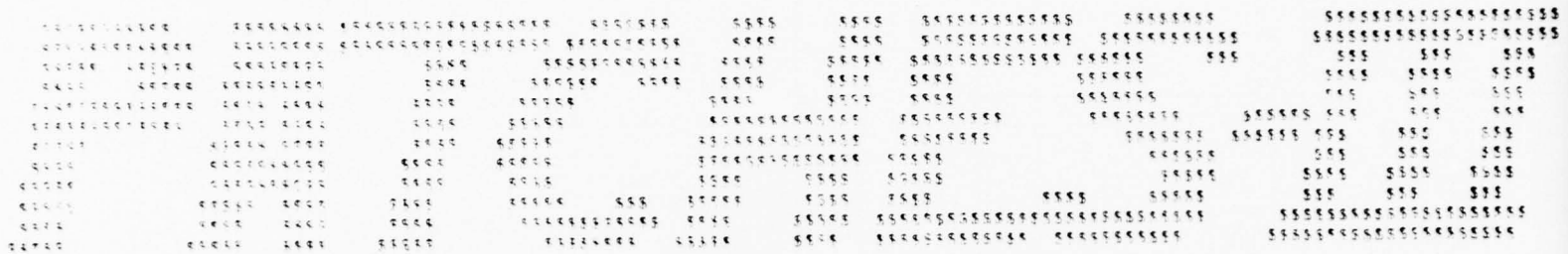

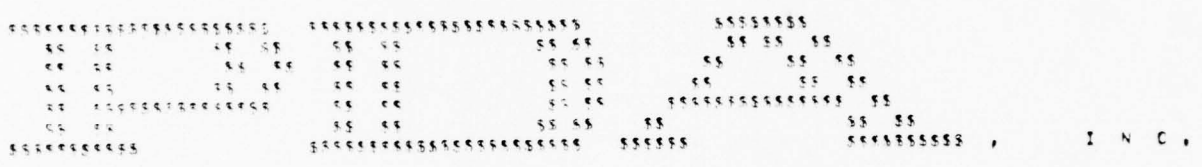

PROTOTYPE DEVELOPMENT ASSOCIATES

VERSION 7.2

BULK DATA CARDS PAGE 1

```
CARD    FIELD-1,FIELD-2,FIELD-3,FIELD-4,FIELD-5,FIELD-6,FIELD-7,FIELD-8,FIELD-9,FIELD-10

  1-    SDC10      10       1        3        5        6        7        8
  2-    SDC10      10       1        2        3        7        6
  3-    SDC10      10       1        1        4        8        7        3
  4-    SDC10           10        1        1        1        5        6        2
  5-    SDC10           10        1        2        1        4        8        5
  6-    SDC10           10        1        3        1        2        3        4
  7-    SDC10           20        1        1        1        5        6        2
  8-    SDC10           20        1        1        4        8        7        3
  9-    SDC10           20        1        2        1        4        8        5
 10-    SDC10           20        1        2        2        3        7        6
 11-    SDC10           20        1        3        1        2        3        4
 12-    SDC1            20        1                 6                          1.24-4
 13-    SDC10           30        1        1        1        5        6        2
 14-    SDC10           30        1        2        1        4        8        5
 15-    SDC10           30        1        2        2        3        7        6
 16-    SDC10           30        1        3        1        2        3        4
 17-    SDC10           30        1        3        5        6        7        8
 18-    SDC1            30        1        7                          1.24-4
 19-    MTRX-15  0.0        .0649857,.0703416  0.10     0.0     .0649857,.0703416  0.10   +X1
 20-    +X1      0.0        .0649857,.0703416  0.10     0.0     .0649857,.0703416  0.10   +X2
 21-    +X2      0.0        .0649857,.0703416  0.10     0.0     .0649857,.0703416  0.10   +X3
 22-    +X3      0.0        .0649857,.0703416  0.10     0.0     .0649857,.0703416  0.10   +X4
 23-    +X4      0.0        .0649857,.0703416  0.10     0.0     .0649857,.0703416  0.10   +X5
 24-    +X5      0.0        .0649857,.0703416  0.10     0.0     .0649857,.0703416  0.10   +X6
 25-    +X6      0.0        .0649857,.0703416  0.10     0.0     .0649857,.0703416  0.10   +X7
 26-    +X7      0.0        .0649857,.0703416  0.10     0.0     .0649857,.0703416  0.10
 27-    MTRX-16  0.0             0.0       0.0       0.0      .0324928,.0324928,.0324928,.0324928+Y1
 28-    +Y1      .0351708,.0351708,.0351708,.0351708  0.05     0.05     0.05     0.05   +Y2
 29-    +Y2      0.0             0.0       0.0       0.0      .0324928,.0324928,.0324928,.0324928+Y3
 30-    +Y3      .0351708,.0351708,.0351708,.0351708  0.05     0.05     0.05     0.05   +Y4
 31-    +Y4      0.0             0.0       0.0       0.0      .0324928,.0324928,.0324928,.0324928+Y5
 32-    +Y5      .0351708,.0351708,.0351708,.0351708  0.05     0.05     0.05     0.05   +Y6
 33-    +Y6      0.0             0.0       0.0       0.0      .0324928,.0324928,.0324928,.0324928+Y7
 34-    +Y7      .0351708,.0351708,.0351708,.0351708  0.05     0.05     0.05     0.05
 35-    MTRX-17  0.0        0.0       0.0       0.0       0.0      0.0      0.0      0.0    +Z1
 36-    +Z1      0.0        0.0       0.0       0.0       0.0      0.0      0.0      0.0    +Z2
 37-    +Z2      .0059704,.0059704,.0059704,.0059704,.0059704,.0059704,.0059704,.0059704+Z3
 38-    +Z3      .0059704,.0059704,.0059704,.0059704,.0059704,.0059704,.0059704,.0059704+Z4
 39-    +Z4      .0064296,.0064296,.0064296,.0064296,.0064296,.0064296,.0064296,.0064296+Z5
 40-    +Z5      .0064296,.0064296,.0064296,.0064296,.0064296,.0064296,.0064296,.0064296+Z6
 41-    +Z6      .0124    .0124    .0124    .0124    .0124    .0124    .0124    .0124    +Z7
 42-    +Z7      .0124    .0124    .0124    .0124    .0124    .0124    .0124    .0124
 43-    MPP             1       15       16       17
 44-    CPDE3           1        1        2        3        4                          +C1
 45-    +C1                      5        6        7        8
 46-    PPDE3           1        1
```

```
CARD    FIELD-1,FIELD-2,FIELD-3,FIELD-4,FIELD-5,FIELD-6,FIELD-7,FIELD-8,FIELD-9,FIELD-10

 47-    MATOR           1       1      64      20
 48-    MTRX-20       101     102     103     104     105     106     107     108+M1
 49-    +M1           109     110     111     112     113     114     115     116+M2
 50-    +M2           117     118     119     120     121     122     123     124+M3
 51-    +M3           125     126     127     128     129     130     131     132+M4
 52-    +M4           133     134     135     136     137     138     139     140+M5
 53-    +M5           141     142     143     144     145     146     147     148+M6
 54-    +M6           149     150     151     152     153     154     155     156+M7
 55-    +M7           157     158     159     160     161     162     163     164
 56-    MATAL           1       1      64      30
 57-    MTRX-30       201     202     203     204     205     206     207     208+A1
 58-    +A1           209     210     211     212     213     214     215     216+A2
 59-    +A2           217     218     219     220     221     222     223     224+A3
 60-    +A3           225     226     227     228     229     230     231     232+A4
 61-    +A4           233     234     235     236     237     238     239     240+A5
 62-    +A5           241     242     243     244     245     246     247     248+A6
 63-    +A6           249     250     251     252     253     254     255     256+A7
 64-    +A7           257     258     259     260     261     262     263     264
 65-    DRATA           5       1       2       3       4                       +D1
 66-    +D1                                                                     +D2
 67-    +D2                                                                   100.
 68-    DRATEQ          6       5       5       6       7       8
 69-    DRATEQ          7       5       4       8       7       3
 70-    DRATEQ          8       5       2       3       7       6
 71-    DHRDP          10       5       6
 72-    TEMP           10       1      10
 73-    MTRX-101,1332+07,4841+07,1332+07,5063-01,1849+00,1840+00,9405+06,5619+06+M10100
 74-    +M10100 ,9405+06
 75-    MTRX-102,1168+07,3767+07,1168+07,7639-01,1759+00,1752+00,7756+06,4951+06+M10200
 76-    +M10200 ,7756+06
 77-    MTRX-103,8639+06,1774+07,8639+06,1242+00,1590+00,1588+00,4693+06,3712+06+M10300
 78-    +M10300 ,4693+06
 79-    MTRX-104,7000+06,7000+06,7000+06,1500+00,1500+00,1500+00,3044+06,3044+06+M10400
 80-    +M10400 ,3044+06
 81-    MTRX-105,1332+07,4841+07,1332+07,5063-01,1849+00,1840+00,9405+06,5619+06+M10500
 82-    +M10500 ,9405+06
 83-    MTRX-106,1211+07,3810+07,1446+07,7874-01,1692+00,1685+00,7929+06,5379+06+M10600
 84-    +M10600 ,8183+06
 85-    MTRX-107,9852+06,1895+07,1659+07,1309+00,1400+00,1397+00,5188+06,4933+06+M10700
 86-    +M10700 ,5915+06
 87-    MTRX-108,8639+06,8639+06,1774+07,1590+00,1242+00,1242+00,3712+06,4693+06+M10800
 88-    +M10800 ,4693+06
 89-    MTRX-109,1332+07,4841+07,1332+07,5063-01,1849+00,1840+00,9405+06,5619+06+M10900
 90-    +M10900 ,9405+06
 91-    MTRX-110,1290+07,3889+07,1963+07,8309-01,1568+00,1561+00,8250+06,6173+06+M11000
 92-    +M11000 ,8977+06
```

```
CARD    FIELD-1,FIELD-2,FIELD-3,FIELD-4,FIELD-5,FIELD-6,FIELD-7,FIELD-8,FIELD-9,FIELD-10
   93-  MTRX-111,.1211+07,.2120+07,.3136+07,.1434+00,.1045+00,.1043+00,.6106+06,.7202+06+M11100
   94-  +M11100 ,.8183+06
   95-  MTRX-112,.1160+07,.1168+07,.3767+07,.1759+00,.7639-01,.7639-01,.4951+06,.7756+06+M11200
   96-  +M11200 ,.7756+06
   97-  MTRX-113,.1332+07,.4841+07,.1332+07,.5063-01,.1849+00,.1840+00,.9405+06,.5619+06+M11300
   98-  +M11300 ,.9405+06
   99-  MTRX-114,.1332+07,.3931+07,.2242+07,.8544-01,.1501+00,.1494+00,.8423+06,.6601+06+M11400
  100-  +M11400 ,.9405+06
  101-  MTRX-115,.1332+07,.2242+07,.3931+07,.1501+00,.8544-01,.8521-01,.6601+06,.8423+06+M11500
  102-  +M11500 ,.9405+06
  103-  MTRX-116,.1332+07,.1332+07,.4841+07,.1849+00,.5063-01,.5063-01,.5619+06,.9405+06+M11600
  104-  +M11600 ,.9405+06
  105-  MTRX-117,.9630+07,.3818+07,.1219+07,.8464-01,.1841+00,.1855+00,.9997+06,.7193+06+M11700
  106-  +M11700 ,.7943+06
  107-  MTRX-118,.9509+07,.3023+07,.1098+07,.1037+00,.1774+00,.1790+00,.8776+06,.6698+06+M11800
  108-  +M11800 ,.6721+06
  109-  MTRX-119,.9284+07,.1546+07,.8721+06,.1392+00,.1649+00,.1668+00,.6507+06,.5780+06+M11900
  110-  +M11900 ,.4453+06
  111-  MTRX-120,.9142+07,.7508+06,.7508+06,.1582+00,.1582+00,.1603+00,.5286+06,.5286+06+M12000
  112-  +M12000 ,.3231+06
  113-  MTRX-121,.7436+07,.3805+07,.1206+07,.8250-01,.1820+00,.1828+00,.9416+06,.6612+06+M12100
  114-  +M12100 ,.7894+06
  115-  MTRX-122,.7358+07,.3052+07,.1363+07,.1039+00,.1686+00,.1696+00,.8368+06,.6545+06+M12200
  116-  +M12200 ,.7100+06
  117-  MTRX-123,.7211+07,.1654+07,.1654+07,.1437+00,.1437+00,.1451+00,.6421+06,.6421+06+M12300
  118-  +M12300 ,.5626+06
  119-  MTRX-124,.7132+07,.9015+06,.1811+07,.1652+00,.1303+00,.1319+00,.5372+06,.6354+06+M12400
  120-  +M12400 ,.4832+06
  121-  MTRX-125,.3382+07,.3781+07,.1181+07,.7853-01,.1780+00,.1779+00,.8337+06,.5533+06+M12500
  122-  +M12500 ,.7804+06
  123-  MTRX-126,.3382+07,.3107+07,.1855+07,.1043+00,.1522+00,.1522+00,.7610+06,.6260+06+M12600
  124-  +M12600 ,.7804+06
  125-  MTRX-127,.3382+07,.1855+07,.3107+07,.1522+00,.1043+00,.1047+00,.6260+06,.7610+06+M12700
  126-  +M12700 ,.7804+06
  127-  MTRX-128,.3382+07,.1181+07,.3781+07,.1780+00,.7853-01,.7907-01,.5533+06,.8337+06+M12800
  128-  +M12800 ,.7804+06
  129-  MTRX-129,.1168+07,.3767+07,.1168+07,.7639-01,.1759+00,.1752+00,.7756+06,.4951+06+M12900
  130-  +M12900 ,.7756+06
  131-  MTRX-130,.1211+07,.3136+07,.2120+07,.1045+00,.1434+00,.1429+00,.7202+06,.6106+06+M13000
  132-  +M13000 ,.8183+06
  133-  MTRX-131,.1290+07,.1963+07,.3889+07,.1568+00,.8309-01,.8292-01,.6173+06,.8250+06+M13100
  134-  +M13100 ,.8977+06
  135-  MTRX-132,.1332+07,.1332+07,.4841+07,.1849+00,.5063-01,.5063-01,.5619+06,.9405+06+M13200
  136-  +M13200 ,.9405+06
  137-  MTRX-133,.2504+08,.1919+07,.1009+07,.1478+00,.1826+00,.1883+00,.1110+07,.1012+07+M13300
  138-  +M13300 ,.5227+06
```

```
CARD    FIELD-1,FIELD-2,FIELD-3,FIELD-4,FIELD-5,FIELD-6,FIELD-7,FIELD-8,FIELD-9,FIELD-10

 139-   MTRX-134,2500+08,1640+07,9664+06,1545+00,1803+00,1860+00,1067+07,9943+06+M13400
 140-   +M13400 ,4800+06
 141-   MTRX-135,2492+08,1123+07,8875+06,1669+00,1759+00,1818+00,9876+06,9622+06+M13500
 142-   +M13500 ,4006+06
 143-   MTRX-136,2488+08,8450+06,8450+06,1736+00,1736+00,1795+00,9448+06,9448+06+M13600
 144-   +M13600 ,3578+06
 145-   MTRX-137,1877+08,1881+07,9713+06,1417+00,1765+00,1807+00,9437+06,8456+06+M13700
 146-   +M13700 ,5089+06
 147-   MTRX-138,1877+08,1645+07,1207+07,1507+00,1675+00,1717+00,9183+06,8710+06+M13800
 148-   +M13800 ,5089+06
 149-   MTRX-139,1877+08,1207+07,1645+07,1675+00,1507+00,1550+00,8710+06,9183+06+M13900
 150-   +M13900 ,5089+06
 151-   MTRX-140,1877+08,9713+06,1881+07,1765+00,1417+00,1461+00,8456+06,9437+06+M14000
 152-   +M14000 ,5089+06
 153-   MTRX-141,7132+07,1811+07,9015+06,1303+00,1652+00,1665+00,6354+06,5372+06+M14100
 154-   +M14100 ,4832+06
 155-   MTRX-142,7211+07,1654+07,1654+07,1437+00,1437+00,1451+00,6421+06,6421+06+M14200
 156-   +M14200 ,5626+06
 157-   MTRX-143,7358+07,1363+07,3052+07,1686+00,1039+00,1054+00,6545+06,8368+06+M14300
 158-   +M14300 ,7100+06
 159-   MTRX-144,7436+07,1206+07,3805+07,1820+00,8250-01,8404-01,6612+06,9416+06+M14400
 160-   +M14400 ,7894+06
 161-   MTRX-145,8639+06,1774+07,8639+06,1242+00,1590+00,1588+00,4693+06,3712+06+M14500
 162-   +M14500 ,4693+06
 163-   MTRX-146,9852+06,1659+07,1895+07,1400+00,1309+00,1308+00,4933+06,5188+06+M14600
 164-   +M14600 ,5915+06
 165-   MTRX-147,1211+07,1446+07,3810+07,1692+00,7874-01,7868-01,5379+06,7929+06+M14700
 166-   +M14700 ,8183+06
 167-   MTRX-148,1332+07,1332+07,4841+07,1849+00,5063-01,5063-01,5619+06,9405+06+M14800
 168-   +M14800 ,9405+06
 169-   MTRX-149,3334+08,8958+06,8958+06,1818+00,1818+00,1898+00,1169+07,1169+07+M14900
 170-   +M14900 ,3765+06
 171-   MTRX-150,3334+08,8958+06,8958+06,1818+00,1818+00,1898+00,1169+07,1169+07+M15000
 172-   +M15000 ,3765+06
 173-   MTRX-151,3334+08,8958+06,8958+06,1818+00,1818+00,1898+00,1169+07,1169+07+M15100
 174-   +M15100 ,3765+06
 175-   MTRX-152,3334+08,8958+06,8958+06,1818+00,1818+00,1898+00,1169+07,1169+07+M15200
 176-   +M15200 ,3765+06
 177-   MTRX-153,2488+08,8450+06,8450+06,1736+00,1736+00,1795+00,9448+06,9448+06+M15300
 178-   +M15300 ,3578+06
 179-   MTRX-154,2492+08,8875+06,1123+07,1759+00,1669+00,1728+00,9622+06,9876+06+M15400
 180-   +M15400 ,4006+06
 181-   MTRX-155,2500+08,9664+06,1640+07,1803+00,1545+00,1604+00,9943+06,1067+07+M15500
 182-   +M15500 ,4800+06
 183-   MTRX-156,2504+08,1009+07,1919+07,1826+00,1478+00,1537+00,1012+07,1110+07+M15600
 184-   +M15600 ,5227+06
```

```
CARD    FIELD-1,FIELD-2,FIELD-3,FIELD-4,FIELD-5,FIELD-6,FIELD-7,FIELD-8,FIELD-9,FIELD-10
  185-  MTRX-157,.9162+07,.750B+06,.750B+06,.1582+00,.1582+00,.1603+00,.5286+06,.5286+06+M15700
  186-  +M15700 ,.3231+06
  187-  MTRX-158,.9284+07,.8721+06,.1546+07,.1649+00,.1392+00,.1412+00,.5780+06,.6507+06+M15800
  188-  +M15800 ,.4453+06
  189-  MTRX-159,.9509+07,.1098+07,.3023+07,.1774+00,.1037+00,.1058+00,.6698+06,.8776+06+M15900
  190-  +M15900 ,.6721+06
  191-  MTRX-160,.9630+07,.1219+07,.3818+07,.1841+00,.8464-01,.8671-01,.7193+06,.9997+06+M16000
  192-  +M16000 ,.7943+06
  193-  MTRX-161,.7000+06,.7000+06,.7000+06,.1500+00,.1500+00,.1500+00,.3044+06,.3044+06+M16100
  194-  +M16100 ,.3044+06
  195-  MTRX-162,.8639+06,.8639+06,.1774+07,.1590+00,.1242+00,.1242+00,.3712+06,.4693+06+M16200
  196-  +M16200 ,.4693+06
  197-  MTRX-163,.1168+07,.1168+07,.3767+07,.1759+00,.7639-01,.7639-01,.4951+06,.7756+06+M16300
  198-  +M16300 ,.7756+06
  199-  MTRX-164,.1332+07,.1332+07,.4841+07,.1849+00,.5063-01,.5063-01,.5619+06,.9405+06+M16400
  200-  +M16400 ,.9405+06
  201-  MTRX-201,.4571-05,.1647-05,.4571-05
  202-  MTRX-202,.4034-05,.1868-05,.4034-05
  203-  MTRX-203,.3037-05,.2279-05,.3037-05
  204-  MTRX-204,.2500-05,.2500-05,.2500-05
  205-  MTRX-205,.4571-05,.1647-05,.4571-05
  206-  MTRX-206,.4173-05,.2007-05,.3977-05
  207-  MTRX-207,.3435-05,.2677-05,.2873-05
  208-  MTRX-208,.3037-05,.3037-05,.2279-05
  209-  MTRX-209,.4571-05,.1647-05,.4571-05
  210-  MTRX-210,.4432-05,.2266-05,.3870-05
  211-  MTRX-211,.4173-05,.3415-05,.2569-05
  212-  MTRX-212,.4034-05,.4034-05,.1868-05
  213-  MTRX-213,.4571-05,.1647-05,.4571-05
  214-  MTRX-214,.4571-05,.2405-05,.3813-05
  215-  MTRX-215,.4571-05,.3813-05,.2405-05
  216-  MTRX-216,.4571-05,.4571-05,.1647-05
  217-  MTRX-217,.3519-05,.2555-05,.4721-05
  218-  MTRX-218,.3121-05,.2719-05,.4323-05
  219-  MTRX-219,.2383-05,.3023-05,.3585-05
  220-  MTRX-220,.1985-05,.3187-05,.3187-05
  221-  MTRX-221,.3053-05,.2377-05,.4543-05
  222-  MTRX-222,.3394-05,.2680-05,.4088-05
  223-  MTRX-223,.2914-05,.3203-05,.3203-05
  224-  MTRX-224,.2655-05,.3506-05,.2788-05
  225-  MTRX-225,.3901-05,.2046-05,.4212-05
  226-  MTRX-226,.3901-05,.2008-05,.3651-05
  227-  MTRX-227,.3901-05,.3651-05,.2008-05
  228-  MTRX-228,.3901-05,.4212-05,.2046-05
  229-  MTRX-229,.4034-05,.1868-05,.4034-05
  230-  MTRX-230,.4173-05,.2569-05,.3415-05
```

```
CARD    FIELD-1,FIELD-2,FIELD-3,FIELD-4,FIELD-5,FIELD-6,FIELD-7,FIELD-8,FIELD-9,FIELD-10
231-    MTRX-231,.4432-05,.3870-05,.2266-05
232-    MTRX-232,.4571-05,.4571-05,.1647-05
233-    MTRX-233,.1565-05,.4241-05,.4999-05
234-    MTRX-234,.1426-05,.4298-05,.4860-05
235-    MTRX-235,.1168-05,.4405-05,.4601-05
236-    MTRX-236,.1028-05,.4462-05,.4462-05
237-    MTRX-237,.1947-05,.3732-05,.4490-05
238-    MTRX-238,.1947-05,.3929-05,.4294-05
239-    MTRX-239,.1947-05,.4294-05,.3929-05
240-    MTRX-240,.1947-05,.4490-05,.3732-05
241-    MTRX-241,.2655-05,.2788-05,.3546-05
242-    MTRX-242,.2914-05,.3243-05,.3243-05
243-    MTRX-243,.3394-05,.4088-05,.2680-05
244-    MTRX-244,.3653-05,.4543-05,.2377-05
245-    MTRX-245,.3037-05,.2279-05,.3037-05
246-    MTRX-246,.3435-05,.2873-05,.2677-05
247-    MTRX-247,.4173-05,.3977-05,.2007-05
248-    MTRX-248,.4571-05,.4571-05,.1647-05
249-    MTRX-249,.5133-06,.5149-05,.5149-05
250-    MTRX-250,.5133-06,.5149-05,.5149-05
251-    MTRX-251,.5133-06,.5149-05,.5149-05
252-    MTRX-252,.5133-06,.5149-05,.5149-05
253-    MTRX-253,.1028-05,.4462-05,.4462-05
254-    MTRX-254,.1168-05,.4601-05,.4405-05
255-    MTRX-255,.1426-05,.4860-05,.4298-05
256-    MTRX-256,.1565-05,.4999-05,.4241-05
257-    MTRX-257,.1985-05,.3187-05,.3187-05
258-    MTRX-258,.2383-05,.3585-05,.3023-05
259-    MTRX-259,.3121-05,.4323-05,.2719-05
260-    MTRX-260,.3519-05,.4721-05,.2555-05
261-    MTRX-261,.2500-05,.2500-05,.2500-05
262-    MTRX-262,.3037-05,.3037-05,.2279-05
263-    MTRX-263,.4034-05,.4034-05,.1868-05
264-    MTRX-264,.4571-05,.4571-05,.1647-05
265-    SPC10     13      1       3       1       5       6       2
266-    SPC10     13      1       2       1       4       8       5
267-    SPC10     13      1       1       1       2       3       4
268-    SPC10     13      1       2       2       3       7       6
269-    SPC1      13      1       6                       .0124-2
270-    SPC1      13      1                       7                       0.1-2
271-    SPC10     12      1       3       1       2       3       4
272-    SPC10     12      1       3       5       6       7       8
273-    SPC10     12      1       1       1       4       8       5
274-    SPC10     12      1       2       1       5       6       2
275-    SPC1      12      1       8                       .05-2
276-    SPC1      12      1                       7                       0.1-2
```

| CARD | FIELD=1 | FIELD=2 | FIELD=3 | FIELD=4 | FIELD=5 | FIELD=6 | FIELD=7 | FIELD=8 | FIELD=9 | FIELD=10 |
|---|---|---|---|---|---|---|---|---|---|---|
| 277= | SPC10 | 23 | 1 | 1 | 1 | 5 | 6 | 2 | | |
| 278= | SPC10 | 23 | 1 | 1 | 4 | 8 | 7 | 3 | | |
| 279= | SPC10 | 23 | 1 | 2 | 1 | 2 | 3 | 4 | | |
| 280= | SPC10 | 23 | 1 | 3 | 1 | 4 | 8 | 5 | | |
| 281= | SPC1 | 23 | 1 | | 6 | | | .0124-2 | | |
| 282= | SPC1 | 23 | 1 | | | 8 | | | .05-2 | |
| 283= | SPC10 | 22 | 1 | 1 | 1 | 5 | 6 | 2 | | |
| 284= | SPC10 | 22 | 1 | 2 | 1 | 4 | 8 | 5 | | |
| 285= | SPC10 | 22 | 1 | 3 | 1 | 2 | 3 | 4 | | |
| 286= | SPC10 | 22 | 1 | 1 | 4 | 8 | 7 | 3 | | |
| 287= | SPC10 | 22 | 1 | 3 | 5 | 6 | 7 | 8 | | |
| 288= | SPC1 | 22 | 1 | | 8 | | | .05-2 | | |
| 289= | ENDDATA | | | | | | | | | |

B U L K  D A T A  C A R D S  PAGE 1

```
CARD    FIELD-1,FIELD-2,FIELD-3,FIELD-4,FIELD-5,FIELD-6,FIELD-7,FIELD-8,FIELD-9,FIELD-10
  1-    CROD3       1       1       1       7       2                                       +C1
  2-    +C1                         4       4       9       5
  3-    CBAR        1       4       4       9       5                                       +A1
  4-    +A1                                                                                 +A2
  5-    +A2                                                                         1.0
  6-    PBARED      2       1       5       9       10      6
  7-    CROD3       2       2       7       8       3                                       +C2
  8-    +C2                         5       9       10      6
  9-    CBEND       1               0.      0.      0.
 10-    PBEND       2               1.0     0.      0.
 11-    MBEND       3               1.77    0.      0.
 12-    CBEND       4               0.      0.      1.68
 13-    PBEND       5               1.      0.      1.68
 14-    MBEND       6               1.77    0.      1.68
 15-    MAT2        1       1                               0.      30.     3
 16-    PBAR        2       2                               0.      30.     3
 17-    MAT1          1     1.+7            .3333333
 18-    PROD3       1       1
 19-    PROD3       2       1
 20-    PLOAD3      10      1       1       1000.
 21-    PLOAD3      10      2       2       1000.
 22-    SPC10       10      1       2       1       2       5       4
 23-    SPC20       10      1       3       1       7       9       4
 24-    SPC10       10      2       2       2       3       6       5
 25-    SPC20       10      2       3       7       8       10      9
 26-    SPC10       10      2       3       2       7       8       3
 27-    PATCHA        1     1       2       5       4                                       +P1
 28-    +P1                                                                                 +P2
 29-    +P2         2.0                             2.0                                     +P3
 30-    +P3                                                                                 +P4
 31-    +P4                         3.36    3.36                                            +P5
 32-    +P5                                                                                 +P6
 33-    PATCHA      2       2       3       6       5                                       +P7
 34-    +P6                                                                                 +P8
 35-    +P7                 1.54    1.54                                                    +P9
 36-    +P8                                                                                 +P10
 37-    +P9                         3.36    3.36
 38-    +P10
 39-    PARAM   PREFL   1.E-8
 40-    ENDDATA
```

```
CARD    FIELD-1,FIELD-2,FIELD-3,FIELD-4,FIELD-5,FIELD-6,FIELD-7,FIELD-8,FIELD-9,FIELD-10

  1-    CPDE3       1       1       1       5       2                               +C
  2-    +C                  4       4       6       3
  3-    GRID        1               0.0     0.0     0.0
  4-    GRID        2               0.125   0.0     0.0
  5-    GRID        3               0.125   0.0     0.125
  6-    GRID        4               0.0     0.0     0.125
  7-    PATCH0      1       1       2       3       4
  8-    MPR         1       1                               0.0     30.0    3
  9-    PATCH       1       1       1       1
 10-    MTRX-1  1.8+6   1.8+6   1.2+6   0.1     0.15    0.15    8.0+5   6.5+5   +M
 11-    +M      6.5+5
 12-    PPDE3       1       1
 13-    SPC10       10      1       3       1       1       5       2
 14-    SPC20       10      1       3       1       2       3       4
 15-    SPC20       10      1       3       1       5       6       4
 16-    DATAG       1               2       1.0     3       1.0     4       1.0     +D
 17-    +D          5       1.0     6       1.0
 18-    DPATO       10      1       2       3       6       5
 19-    DPATO       20      1       4       4       6       3
 20-    PLOAD3      10      1       10      -4.0+3
 21-    PLOAD3      10      1       20      -4.0+3
 22-    END DATA
```



ATJ-S Bar Specimen
Bulk Data Model

REPORT DISTRIBUTION

PART 1 - GOVERNMENT

Administrative & Liaison Activities

Chief of Naval Research
Department of the Navy
Arlington, Virginia 22217
Attn: Code 474 (2)
471
222

Assistant Chief for Technology
Office of Naval Research, Code 200
Arlington, Virginia 22217

Director
ONR Branch Office
495 Summer Street
Boston, Massachusetts 02210

Director
ONR Branch Office
219 S. Dearborn Street
Chicago, Illinois 60604

Director
Naval Research Laboratory
Attn: Code 2629 (ONRL)
Washington, D.C. 20390 (6)

U.S. Naval Research Laboratory
Attn: Code 2627
Washington, D.C. 20390

Director
ONR - New York Area Office
715 Broadway - 5th Floor
New York, N.Y. 10003

Director
ONR Branch Office
1030 E. Green Street
Pasadena, California 91101

Defense Documentation Center
Cameron Station
Alexandria, Virginia 22314 (12)

Army

Commanding Officer
U.S. Army Research Office Durham
Attn: Mr. J. J. Murray
CRD-AA-IP
Box CM, Duke Station
Durham, North Carolina 27706 (2)

Commanding Officer
AMMXMR-ATL
Attn: Mr. R. Shea
U.S. Army Materials Res. Agency
Watertown, Massachusetts 02172

Watervliet Arsenal
MAGGS Research Center
Watervliet, New York 12189
Attn: Director of Research

Technical Library

Redstone Scientific Info. Center
Chief, Document Section
U.S. Army Missile Command
Redstone Arsenal, Alabama 35809

Army R&D Center
Fort Belvoir, Virginia 22060

Navy

Commanding Officer and Director
Naval Ship Research & Development Center
Bethesda, Maryland 20034
Attn: Code 042 (Tech. Lib. Br.)
17 (Struc. Mech. Lab.)
172
174
177
1800 (Appl. Math. Lab.)

Commanding Officer and Director
Naval Ship Research & Development Center
Bethesda, Maryland 20034
Attn: Code 5412S (Dr. W. D. Sette)
19 (Dr. M. M. Sevik)
1901 (Dr. M. Strassberg)
1945
196 (Dr. D. Feit)
1962

Naval Weapons Laboratory
Dahlgren, Virginia 22448

Naval Research Laboratory
Washington, D.C. 20375
Attn: Code 8400
8410
8430
8440
6300
6390
6380

Undersea Explosion Research Division
Naval Ship R&D Center
Norfolk Naval Shipyard
Portsmouth, Virginia 23709
Attn: Dr. E. Palmer - Code 780

Naval Ship Research & Development Center
Annapolis Division
Annapolis, Maryland 21402
Attn: Code 2740 - Dr. Y. F. Wang
28 - Mr. R. J. Wolfe
281 - Mr. R. B. Niederberger
2814 - Dr. H. Vanderveldt

Technical Library
Naval Underwater Weapons Center
Pasadena Annex
3202 E. Foothill Blvd.
Pasadena, California 91107

U.S. Naval Weapons Center
China Lake, California 93557
Attn: Code 4062 - Mr. W. Werback
4520 - Mr. Ken Bischel

Commanding Officer
U.S. Naval Civil Engr. Lab.
Code L31
Port Hueneme, California 93041

Technical Director
U.S. Naval Ordnance Laboratory
White Oak
Silver Spring, Maryland 20910

Technical Director
Naval Undersea R&D Center
San Diego, California 92132

Supervisor of Shipbuilding
U.S. Navy
Newport News, Virginia 23607

Technical Director
Mare Island Naval Shipyard
Vallejo, California 94592

U.S. Navy Underwater Sound Ref. Lab.
Office of Naval Research
P.O. Box 8337
Orlando, Florida 32806

Chief of Naval Operations
Dept. of the Navy
Washington, D.C. 20350
Attn: Code Op07T

Strategic Systems Project Office
Department of the Navy
Washington, D.C. 20390
Attn: NSP-001 Chief Scientist

Deep Submergence Systems
Naval Ship Systems Command
Code 39522
Department of the Navy
Washington, D.C. 20360

Engineering Dept.
U.S. Naval Academy
Annapolis, Maryland 21402

Naval Air Systems Command
Dept. of the Navy
Washington, D.C. 20360
Attn: NAVAIR 5302 Aero & Structures
5308 Structures
52031F Materials
604 Tech. Library
320B Structures

Director, Aero Mechanics
Naval Air Development Center
Johnsville
Warminster, Pennsylvania 18974

Naval Facilities Engineering Command
Dept. of the Navy
Washington, D.C. 20360
Attn: NAVFAC 03 Research & Dev.
04 Research & Dev.
14114 Tech. Library

Naval Sea Systems Command
Dept. of the Navy
Washington, D.C. 20360
Attn: NAVSHIP 03 Res. & Technology
031 Ch. Scientist for R&D
03412 Hydromechanics
037 Ship Silencing Div.
035 Weapons Dynamics

Naval Ship Engineering Center
Prince George's Plaza
Hyattsville, Maryland 20782
Attn: NAVSEC 6100 Ship Sys Engr & Des Dep
6102C Computer-Aided Ship Des
6105G
6110 Ship Concept Design
6120 Hull Div.
6120D Hull Div.
6128 Surface Ship Struct.
6129 Submarine Struct.

Air Force

Commander WADD
Wright-Patterson Air Force Base
Dayton, Ohio 45433
Attn: Code WWRMDD
AFFDL (FDDS)
Structures Division
AFLC (MCEEA)

Chief, Applied Mechanics Group
U.S. Air Force Inst. of Tech.
Wright-Patterson Air Force Base
Dayton, Ohio 45433

Chief, Civil Engineering Branch
WLRC, Research Division
Air Force Weapons Laboratory
Kirtland AFB, New Mexico 87117

Air Force Office of Scientific Research
1400 Wilson Blvd.
Arlington, Virginia 22209
Attn: Mechanics Div.

NASA

Structures Research Division
National Aeronautics & Space Admin.
Langley Research Center
Langley Station
Hampton, Virginia 23365

National Aeronautic & Space Admin.
Associate Administrator for Advanced
Research & Technology
Washington, D.C. 02546

Scientific & Tech. Info. Facility
NASA Representative (S-AK/DL)
P.O. Box 5700
Bethesda, Maryland 20014

Other Government Activities

Commandant
Chief, Testing & Development Div.
U.S. Coast Guard
1300 E. Street, N.W.
Washington, D.C. 20226

Technical Director
Marine Corps Dev. & Educ. Command
Quantico, Virginia 22134

Director
National Bureau of Standards
Washington, D.C. 20234
Attn: Mr. B. L. Wilson, EM 219

Dr. M. Gaus
National Science Foundation
Engineering Division
Washington, D.C. 20550

Science & Tech. Division
Library of Congress
Washington, D.C. 20540

Director
Defense Nuclear Agency
Washington, D.C. 20305
Attn: SPSS

Commander Field Command
Defense Nuclear Agency
Sandia Base
Albuquerque, New Mexico 87115

Director Defense Research & Engrg
Technical Library
Room 3C-128
The Pentagon
Washington, D.C. 20301

Chief, Airframe & Equipment Branch
FS-120
Office of Flight Standards
Federal Aviation Agency
Washington, D.C. 20553

Chief, Research and Development
Maritime Administration
Washington, D.C. 20235

Deputy Chief, Office of Ship Constr.
Maritime Administration
Washington, D.C. 20235
Attn: Mr. U. L. Russo

Atomic Energy Commission
Div. of Reactor Devel. & Tech.
Germantown, Maryland 20767

Ship Hull Research Committee
National Research Council
National Academy of Sciences
2101 Constitution Avenue
Washington, D.C. 20418
Attn: Mr. A. R. Lytle

PART 2 - CONTRACTORS AND OTHER TECHNICAL COLLABORATORS

Universities

Dr. J. Tinsley Oden
University of Texas at Austin
345 Eng. Science Bldg.
Austin, Texas 78712

Prof. Julius Miklowitz
California Institute of Technology
Div. of Engineering & Applied Sciences
Pasadena, California 91109

Dr. Harold Liebowitz, Dean
School of Engr. & Applied Science
George Washington University
725 - 23rd St., N.W.
Washington, D.C. 20006

Prof. Eli Sternberg
California Institute of Technology
Div. of Engr. & Applied Sciences
Pasadena, California 91109

Prof. Paul M. Naghdi
University of California
Div. of Applied Mechanics
Etcheverry Hall
Berkeley, California 94720

Professor P. S. Symonds
Brown University
Division of Engineering
Providence, R.I. 02912

Prof. A. J. Durelli
The Catholic University of America
Civil/Mechanical Engineering
Washington, D.C. 20017

Prof. R. B. Testa
Columbia University
Dept. of Civil Engineering
S. W. Mudd Bldg.
New York, N.Y. 10027

Prof. H. H. Bleich
Columbia University
Dept. of Civil Engineering
Amsterdam & 120th St.
New York, N.Y. 10027

Prof. F. L. DiMaggio
Columbia University
Dept. of Civil Engineering
616 Mudd Building
New York, N.Y. 10027

Prof. A. M. Freudenthal
George Washington University
School of Engineering &
Applied Science
Washington, D.C. 20006

D. C. Evans
University of Utah
Computer Science Division
Salt Lake City, Utah 84112

Prof. Norman Jones
Massachusetts Inst. of Technology
Dept. of Naval Architecture &
Marine Engr.
Cambridge, Massachusetts 02139

Prof. Albert I. King
Biomechanics Research Center
Wayne State University
Detroit, Michigan 48202

Dr. V. R. Hodgson
Wayne State University
School of Medicine
Detroit, Michigan 48202

Dean B. A. Boley
Northwestern University
Technological Institute
2145 Sheridan Road
Evanston, Illinois 60201

Prof. P. G. Hodge, Jr.
University of Minnesota
Dept. of Aerospace Engr. & Mechanics
Minneapolis, Minnesota 55455

Dr. D. C. Drucker
University of Illinois
Dean of Engineering
Urbana, Illinois 61801

Prof. N. M. Newmark
University of Illinois
Dept. of Civil Engineering
Urbana, Illinois 61801

Prof. E. Reissner
University of California, San Diego
Dept. of Applied Mechanics
La Jolla, California 92037

Prof. William A. Nash
University of Massachusetts
Dept. of Mechanics & Aerospace Engr.
Amherst, Massachusetts 01002

Library (Code 0384)
U.S. Naval Postgraduate School
Monterey, California 93940

Prof. Arnold Allentuch
Newark College of Engineering
Dept. of Mechanical Engineering
323 High Street
Newark, New Jersey 07102

Dr. George Herrmann
Stanford University
Dept. of Applied Mechanics
Stanford, California 94305

Prof. J. D. Achenbach
Northwestern University
Dept. of Civil Engineering
Evanston, Illinois 60201

Director, Applied Research Lab.
Pennsylvania State University
P.O. Box 30
State College, Pennsylvania 16801

Prof. Eugene J. Skudrzyk
Pennsylvania State University
Applied Research Laboratory
Dept. of Physics - P.O. Box 30
State College, Pennsylvania 16801

Prof. J. Kempner
Polytechnic Institute of Brooklyn
Dept. of Aero. Engrg. & Applied Mech.
333 Jay Street
Brooklyn, N.Y. 11201

Prof. J. Klosner
Polytechnic Institute of Brooklyn
Dept. of Aerospace & Appl. Mech.
333 Jay Street
Brooklyn, N.Y. 11201

Prof. R. A. Schapery
Texas A&M University
Dept. of Civil Engineering
College Station, Texas 77840

Prof. W. D. Pilkey
University of Virginia
Dept. of Aerospace Engineering
Charlottesville, Virginia 22903

Dr. H. G. Schaeffer
University of Maryland
Aerospace Engineering Dept.
College Park, Maryland 20742

Prof. K. D. Willmert
Clarkson College of Technology
Dept. of Mechanical Engineering
Potsdam, N.Y. 13676

Dr. J. A. Stricklin
Texas A&M University
Aerospace Engineering Dept.
College Station, Texas 77843

Dr. L. A. Schmit
University of California, L.A.
School of Engineering & Applied Science
Los Angeles, California 90024

Dr. H. A. Kamel
The University of Arizona
Aerospace & Mech. Engineering Dept.
Tucson, Arizona 85721

Dr. B. S. Berger
University of Maryland
Dept. of Mechanical Engineering
College Park, Maryland 20742

Prof. G. R. Irwin
Dept. of Mechanical Engrg.
University of Maryland
College Park, Maryland 20742

Dr. S. J. Fenves
Carnegie-Mellon University
Dept. of Civil Engineering
Schenley Park
Pittsburgh, Pennsylvania 15213

Dr. Ronald L. Huston
Dept. of Engineering Analysis
Mail Box 112
University of Cincinnati
Cincinnati, Ohio 45221

Prof. George Sih
Dept. of Mechanics
Lehigh University
Bethlehem, Pennsylvania 18015

Prof. A. S. Kobayashi
University of Washington
Dept. of Mechanical Engineering
Seattle, Washington 98105

Librarian
Webb Institute of Naval Architecture
Crescent Beach Road, Glen Cove
Long Island, New York 11542

Prof. Daniel Frederick
Virginia Polytechnic Institute
Dept. of Engineering Mechanics
Blacksburg, Virginia 24061

Prof. A. C. Eringen
Dept. of Aerospace & Mech. Sciences
Princeton University
Princeton, New Jersey 08540

Dr. S. L. Koh
School of Aero., Astro. & Engr. Sc.
Purdue University
Lafayette, Indiana 47907

Prof. E. H. Lee
Div. of Engrg. Mechanics
Stanford University
Stanford, California 94305

Prof. R. D. Mindlin
Dept. of Civil Engrg.
Columbia University
S. W. Mudd Building
New York, N.Y. 10027

Prof. S. B. Dong
University of California
Dept. of Mechanics
Los Angeles, California 90024

Prof. Burt Paul
University of Pennsylvania
Towne School of Civil & Mech. Engrg.
Rm. 113 - Towne Building
220 S. 33rd Street
Philadelphia, Pennsylvania 19104

Prof. H. W. Liu
Dept. of Chemical Engr. & Metal.
Syracuse University
Syracuse, N.Y. 13210

Prof. S. Bodner
Technion R&D Foundation
Haifa, Israel

Prof. R. J. H. Bollard
Chairman, Aeronautical Engr. Dept.
207 Guggenheim Hall
University of Washington
Seattle, Washington 98105

Prof. G. S. Heller
Division of Engineering
Brown University
Providence, Rhode Island 02912

Prof. Werner Goldsmith
Dept. of Mechanical Engineering
Div. of Applied Mechanics
University of California
Berkeley, California 94720

Prof. J. R. Rice
Division of Engineering
Brown University
Providence, Rhode Island 02912

Prof. R. S. Rivlin
Center for the Application of Mathematics
Lehigh University
Bethlehem, Pennsylvania 18015

Library (Code 0384)
U. S. Naval Postgraduate School
Monterey, California 93940

Dr. Francis Cozzarelli
Div. of Interdisciplinary
Studies & Research
School of Engineering
State University of New York
Buffalo, N. Y. 14214

Industry and Research Institutes

Library Services Department
Report Section Bldg. 14-14
Argonne National Laboratory
9700 S. Cass Avenue
Argonne, Illinois 60440

Dr. M. C. Junger
Cambridge Acoustical Associates
129 Mount Auburn St.
Cambridge, Massachusetts 02138

Dr. L. H. Chen
General Dynamics Corporation
Electric Boat Division
Groton, Connecticut 06340

Dr. J. E. Greenspon
J. G. Engineering Research Associates
3831 Menlo Drive
Baltimore, Maryland 21215

Dr. S. Batdorf
The Aerospace Corp.
P. O. Box 92957
Los Angeles, California 90009

Dr. K. C. Park
Lockheed Palo Alto Research Laboratory
Dept. 5233, Bldg. 205
3251 Hanover Street
Palo Alto, California 94304

Library
Newport News Shipbuilding &
Dry Dock Company
Newport News, Virginia 23607

Dr. W. F. Bozich
McDonnell Douglas Corporation
5301 Bolsa Avenue
Huntington Beach, California 92647

Dr. H. N. Abramson
Southwest Research Institute
Technical Vice President
Mechanical Sciences
P. O. Drawer 28510
San Antonio, Texas 78284

Dr. R. C. DeHart
Southwest Research Institute
Dept. of Structural Research
P. O. Drawer 28510
San Antonio, Texas 78284

Dr. M. L. Baron
Weidlinger Associates, Consulting
Engineers
110 East 59th Street
New York, N. Y. 10022

Dr. W. A. von Riesemann
Sandia Laboratories
Sandia Base
Albuquerque, New Mexico 87115

Dr. T. L. Geers
Lockheed Missiles & Space Co.
Palo Alto Research Laboratory
3251 Hanover Street
Palo Alto, California 94304

Dr. J. L. Tocher
Boeing Computer Services, Inc.
P.O. Box 24346
Seattle, Washington 98124

Mr. William Caywood
Code BBE, Applied Physics Laboratory
9621 Georgia Avenue
Silver Spring, Maryland 20034

Mr. P. C. Durup
Lockheed-California Company
Aeromechanics Dept., 74-43
Burbank, California 91503

Unclassified

SECURITY CLASSIFICATION OF THIS PAGE (When Data Entered)

| REPORT DOCUMENTATION PAGE | READ INSTRUCTIONS BEFORE COMPLETING FORM |
|---|---|
| 1. REPORT NUMBER: PDA-TR 1045-00 | 2. GOVT ACCESSION NO. / 3. RECIPIENT'S CATALOG NUMBER |
| 4. TITLE (and Subtitle): A General Three-Dimensional Computational Model for Nonlinear Composite Structures and Materials. | 5. TYPE OF REPORT & PERIOD COVERED: FINAL REPORT, October 75 - October 76 / 6. PERFORMING ORG. REPORT NUMBER |
| 7. AUTHOR(s): Edward L. Stanton | 8. CONTRACT OR GRANT NUMBER(s): N00014-76-C-0161 |
| 9. PERFORMING ORGANIZATION NAME AND ADDRESS: Prototype Development Associates, 1740 Garry Avenue, Suite 201, Santa Ana, California 92705 | 10. PROGRAM ELEMENT, PROJECT, TASK AREA & WORK UNIT NUMBERS |
| 11. CONTROLLING OFFICE NAME AND ADDRESS: Office of Naval Research, 800 N. Quincy Street, Arlington, Virginia 22217 | 12. REPORT DATE: June 1977 / 13. NUMBER OF PAGES: 126 |
| 14. MONITORING AGENCY NAME & ADDRESS (if different from Controlling Office) | 15. SECURITY CLASS (of this report): UNCLASSIFIED / 15a. DECLASSIFICATION DOWNGRADING SCHEDULE |

16. DISTRIBUTION STATEMENT (of this Report)

Approved for public release; distribution unlimited.

17. DISTRIBUTION STATEMENT (of the abstract entered in Block 20, if different from Report)

18. SUPPLEMENTARY NOTES

19. KEY WORDS (Continue on reverse side if necessary and identify by block number)

Nonlinear Composite Materials
Triaxial Stress Analysis
3D Isoparametric Finite Elements
Carbon-Carbon Composites
Solid Geometry Modeling

20. ABSTRACT (Continue on reverse side if necessary and identify by block number)

A computational model for the analysis of structural and microstructural behavior in general solids of composite material is presented. Emphasis is placed on representing the anomalous material behavior of composites and on the construction of computational models with variable properties. Alternative material models using continuum and statistical mechanics were reviewed and a modular code designed for compatibility with several different models. The constituent materials

DD FORM 1 JAN 73 1473 EDITION OF 1 NOV 65 IS OBSOLETE

Unclassified

SECURITY CLASSIFICATION OF THIS PAGE (When Data Entered)

390714

are characterized in terms of those state variables that correlate a materials response such as effective stress or strain energy. A parametric cubic representation is used for all state variables, the solid geometry and all physical properties. The associated finite element extends isoparametric modeling to allow properties, linear or nonlinear, to vary over the volume of an element as in rosette material construction. Applications of the model to a carbon-carbon unit cell, to strain singularities and to the inelastic response of a graphite bar illustrate its utility. Good agreement with triaxial test data for inelastic strains under hydrostatic pressure is obtained. Numerical results are computed using PATCHES-III and the conjugate gradient algorithm without the assembly of large matrices. This approach is tailored for vector processors and can reduce the high cost of nonlinear three-dimensional analyses.